NEUROSCIENCE

# Phosphorylation-dependent positive feedback on the oxytocin receptor through the kinase PKD1 contributes to long-term social memory

**Fei Wang[1,2]†, Xiang-Sha Yin[1]†, Jie Lu[1], Cheng Cen[1]*, Yun Wang[1,3]***



**Social memory enables one to recognize and distinguish specific individuals. It is fundamental to social behaviors that can be mediated by the oxytocin receptor (OXTR), such as forming relationships. We investigated the molecular regulation and function of OXTR in animal behavior involving social memory. We found that Ser$^{261}$ in OXTR was phosphorylated by protein kinase D1 (PKD1). Neuronal $Ca^{2+}$ signaling and behavior analyses revealed that rats expressing a mutated form of OXTR that cannot be phosphorylated at this residue (OXTR S261A) in the medial amygdala (MeA) exhibited impaired long-term social memory (LTSM). Blocking the phosphorylation of wild-type OXTR in the MeA using an interfering peptide in rats or through conditional knockout of *Pkd1* in mice reduced social memory retention, whereas expression of a phosphomimetic mutant of OXTR rescued it. In HEK293A cells, the PKD1-mediated phosphorylation of OXTR promoted its binding to $G_q$ protein and, in turn, OXTR-mediated phosphorylation of PKD1, indicating a positive feedback loop. In addition, OXTR with a single-nucleotide polymorphism found in humans (rs200362197), which has a mutation in the conserved recognition region in the PKD1 phosphorylation site, showed impaired activation and signaling in vitro and in HEK293A cells similar to that of the S216A mutant. Our findings describe a phosphoregulatory loop for OXTR and its critical role in social behavior that might be further explored in associated disorders.**

## INTRODUCTION

Abnormal social behavior is associated with various neurological conditions, such as autism spectrum disorder and schizophrenia (*1*, *2*). Among various types of social behaviors, social memory—the ability to recognize familiar conspecifics—is a prerequisite for exhibiting appropriate behaviors, such as aggression, avoidance, cooperative behavior, and even mating behavior, toward others (*3*, *4*). The hormone oxytocin (OXT) and its receptor (OXTR) are widely expressed in brain regions associated with networks that play a major role in regulating social behaviors and emotions (*5*–*9*).

OXTR is a G protein–coupled receptor (GPCR) that couples to $G_q$ to mediate OXT signaling in the adult brain (*10*–*13*). Subsequent to OXTR activation, $G_q$ activates the mitogen-activated protein kinase (MAPK) cascade, leading to the phosphorylation of the transcription factor cyclic adenosine monophosphate response element–binding protein, activation of new protein synthesis, enhanced long-term potentiation, and elicitation of behavioral responses (*14*, *15*). The activity and function of GPCRs can be regulated by diverse post-translational modifications that can modulate the structure, function, and pharmacology of the receptors (*16*, *17*). OXTR is phosphorylated in the brain, but the functional and biological consequences of this modification, especially in vivo, is unclear (*11*).

The protein kinase D (PKD) belongs to serine/threonine protein kinase family, which includes three isoforms (*18*). In the nervous system, PKD1 regulates Golgi function, neuronal polarity, and dendritic development (*19*–*22*). We previously reported that the phosphorylation of N-cadherin by PKD1 promotes functional synapse formation and regulates learning and memory (*23*). Sequence alignment reveals that OXTR has a consensus phosphorylation sequence recognized by PKD1. In this study, using a breadth of in vitro assays and cellular and in vivo models, we investigated whether PKD1 phosphorylates OXTR and whether this mechanism is involved in the maintenance of long-term social memory (LTSM).

## RESULTS

### PKD1 phosphorylates the OXTR at Ser$^{261}$, activating downstream MAPK signaling

The consensus phosphorylation site of the PKD family is a serine residue with an L/V/I residue (Leu, Val, or Ile) at position −5 and R/K (Arg or Lys) at position −3 (*24*). By means of bioinformatics, we initially found a PKD target sequence (LARVS) before the Ser$^{261}$ site on the OXTR. To verify the potential phosphorylation of this site, we first generated truncated glutathione *S*-transferase (GST)–tagged constructs of the third intracellular loop (IL3) and the C terminus of the rat OXTR and conducted in vitro kinase assays. The results showed that PKD1 phosphorylates the IL3 of OXTR but not its C terminus. Phosphorylation was abolished when Ser$^{261}$ was mutated to alanine (S261A) (Fig. 1A and fig. S1A). The above results indicate that PKD1 can phosphorylate OXTR in its IL3 at Ser$^{261}$.

We further explored the interactions between the OXTR and PKD1, and in vitro pull-down experiments showed direct binding between purified His-PKD1 and GST-OXTR-IL3. In contrast, the S261A mutation did not interfere with the binding between the OXTR and PKD1 (fig. S1B). The ratio of phosphorylated extracellular signal–related kinase 1 and 2 (p-ERK1/2) relative to the total abundance of ERK1/2 was significantly increased after 5 min of OXT incubation at a final concentration of 50 nM (fig. S1C). Therefore,

[1]Department of Neurobiology, School of Basic Medical Sciences and Neuroscience Research Institute; Key Lab for Neuroscience, Ministry of Education of China and National Health Commission and State Key Laboratory of Natural and Biomimetic Drugs, Peking University, Beijing 100083, China. [2]Department of Neurology, Xuanwu Hospital, Capital Medical University, Beijing 100053, China. [3]PKU-IDG/McGovern Institute for Brain Research, Peking University, Beijing 100871, China.
*Corresponding author. Email: wangy66@bjmu.edu.cn (Y.W.); cencheng418@163.com (C.C.)
†These authors contributed equally to this work.

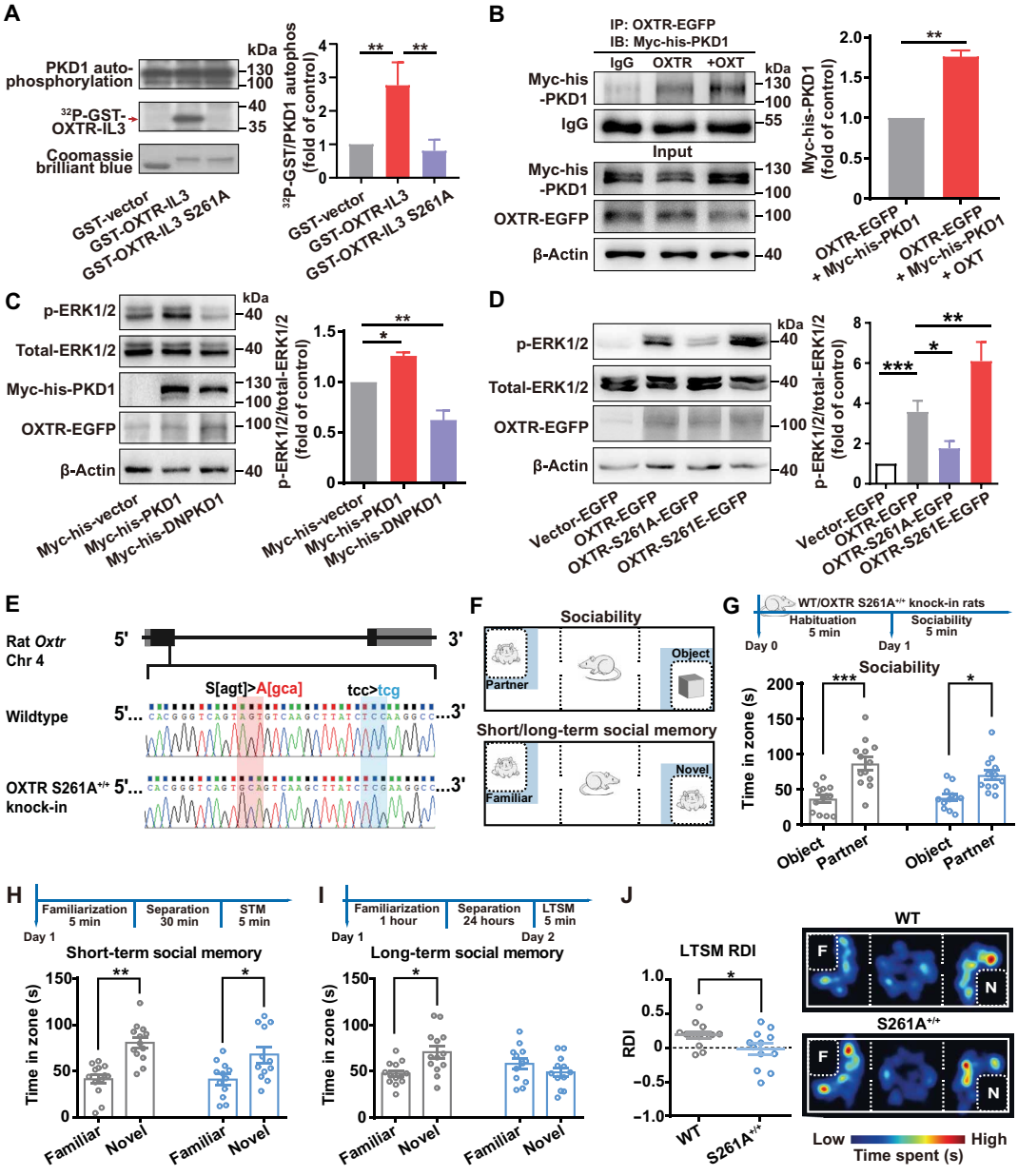


**Fig. 1. Phosphorylation of OXTR at Ser$^{261}$ by PKD1 has an impact on LTSM.** (**A**) Representative Western blot and autoradiogram for in vitro kinase assay with purified recombinant human PKD1 and GST-vector, GST-OXTR-IL3, and GST-OXTR-IL3 S261A. The red arrow indicates the location of phosphorylated GST-OXTR-IL3. Data are means ± SEM from $n = 3$ independent experiments, analyzed by one-way ANOVA with Tukey's post hoc test, $^{**}P < 0.01$. (**B**) Representative immunoblot (IB) of PKD1 coimmunoprecipitated with OXTR (IP) in HEK293 cells transfected with myc-his-PKD1 and OXTR-EGFP, with or without OXT treatment. Data are means ± SEM from $n = 3$ independent experiments. Unpaired $t$ test with Welch's correction, $^{**}P < 0.01$. IgG, immunoglobulin G. (**C**) Representative Western blot of p-ERK1/2 and total-ER1/2 in HEK293 cells transfected with myc-his-vector, myc-his-PKD1, myc-his-DNPKD1, and OXTR-EGFP after OXT treatment. Data are means ± SEM from $n = 4$ independent experiments. One-way ANOVA with Tukey's post hoc test, $^{*}P < 0.05$, $^{**}P < 0.01$. (**D**) Representative Western blot of p-ERK1/2 and total-ER1/2 in HEK293 cells transfected with myc-his-vector, vector-EGFP, OXTR-EGFP, OXTR-S261A-EGFP, and OXTR-S261E-EGFP after OXT treatment. Data are means ± SEM from $n = 4$ independent experiments. One-way ANOVA with Tukey's post hoc test, $^{*}P < 0.05$, $^{**}P < 0.01$, $^{***}P < 0.001$. (**E**) Schematic diagram of OXTR S261A$^{+/+}$ knock-in rats. (**F**) Diagram of the sociability and social discrimination test. The blue shadows represent the ROIs in which the time in zone is counted. (**G**) Top: Sociability protocol. Bottom: Time spent by WT (gray) and OXTR S261A$^{+/+}$ (blue) rats in zones around the partner or around the object. Data are means ± SEM from $n = 13$ and 12 animals, respectively. Two-way repeated-measures ANOVA, Genotype × Social stimulus interaction: $F_{1,23} = 2.782$, $P = 0.109$. Genotype: $F_{1,23} = 1.987$, $P = 0.172$. Social stimulus: $F_{1,23} = 38.71$, $P < 0.001$. Sidak's post hoc test, $^{*}P < 0.05$, $^{***}P < 0.001$. (**H**) Top: Short-term social memory (STSM) protocol. Bottom: Time spent by WT (gray) and OXTR S261A$^{+/+}$ (blue) rats in zones around the novel juvenile or around the familiar one. Data are means ± SEM from $n = 13$ and 12 animals, respectively. Two-way repeated-measures ANOVA, Genotype × Social stimulus interaction: $F_{1,23} = 0.743$, $P = 0.397$. Genotype: $F_{1,23} = 2.264$, $P = 0.146$. Social stimulus: $F_{1,23} = 19.66$, $P < 0.001$. Sidak's post hoc test, $^{*}P < 0.05$, $^{**}P < 0.01$. (**I**) Top: Long-term social memory (LTSM) protocol. Bottom: Time spent by WT (gray) and OXTR S261A$^{+/+}$ (blue) rats in zones around the novel juvenile or around the familiar one. Data are means ± SEM from $n = 13$ and 12 animals, respectively. Two-way repeated-measures ANOVA, Genotype × Social stimulus interaction: $F_{1,23} = 0.756$, $P < 0.05$. Genotype: $F_{1,23} = 1.478$, $P = 0.236$. Social stimulus: $F_{1,23} = 1.401$, $P = 0.248$. Sidak's post hoc test, $^{*}P < 0.05$. (**J**) Left: LTSM RDI of WT (gray, $n = 13$) versus OXTR S261A$^{+/+}$ (blue, $n = 12$) rats. Unpaired $t$ test, $^{*}P < 0.05$. Right: Representative heatmap of WT and OXTR S261A$^{+/+}$ rats during LTSM testing. RDI, relative duration of investigation.

we used 50 nM and 5 min as the OXT stimulation conditions for the subsequent cell experiments. In the coimmunoprecipitation of PKD1 and OXTR, the binding was enhanced after OXT stimulation, indicating that the interaction between PKD1 and OXTR was affected by OXTR activation (Fig. 1B).

To validate that the activity of PKD1 plays a role in the OXTR pathway, we overexpressed wild-type (WT) PKD1 (Myc-his-PKD1) and dominant-negative PKD1 [Myc-his-DNPKD1 (D727A)] (*25*) in human embryonic kidney (HEK) 293A cells stimulated with OXT. The results showed that p-ERK1/2 significantly increased after

PKD1 overexpression and decreased with DNPKD1 (Fig. 1C). To confirm the importance of OXTR phosphorylation at $Ser^{261}$, we overexpressed OXTR–enhanced green fluorescent protein (EGFP), OXTR-S261A-EGFP, and OXTR-S261E-EGFP (in which the $Ser^{261}$ site of the OXTR is mutated to glutamate to mimic a sustained phosphorylation state) in HEK293A cells and treated with OXT. We found that the overexpression of OXTR-EGFP induced a significant increase in p-ERK1/2 compared with that induced by vector-EGFP, whereas p-ERK1/2 significantly decreased in cells expressing OXTR-S261A-EGFP and was increased in cells expressing OXTR-S261E EGFP compared to those expressing OXTR-EGFP (Fig. 1D). Together, the PKD1-mediated phosphorylation of the OXTR at $Ser^{261}$ increases the activity of OXTR downstream signaling after OXT stimulation. Basal conditions (without incubation with OXT) showed no statistically significant change in p-ERK1/2 levels (fig. S1, D and E). Therefore, the modulation of OXTR pathway activation by the phosphorylation of OXTR at $Ser^{261}$ by PKD1 depends on OXTR activation.

## Abolishing the phosphorylation of OXTR at $Ser^{261}$ impairs LTSM

We then explored whether the phosphorylation process affects animal behaviors. A line of Sprague-Dawley rats carrying a mutation in the site (OXTR $S261A^{+/+}$) was developed by CRISPR/Cas–mediated genome engineering. The S261A (AGT to GCA) mutation was introduced into the *Oxtr* gene (Fig. 1E).

The OXTR is involved in various social-related behaviors, such as social cognition, emotion, aggression, and affiliation behaviors (*26*). We tested these behavioral phenotypes in OXTR $S261A^{+/+}$ knock-in rats. The social behavior of OXTR $S261A^{+/+}$ rats was assessed by social discrimination tests, which consisted of sociability, short-term social memory (STSM), and LTSM protocols (Fig. 1F). The sociability and STSM of OXTR $S261A^{+/+}$ rats were consistent with that of WT rats. The animals all preferred to interact with the partner than with the object (Fig. 1G) and preferred to interact with the novel juvenile rather than with the familiar one after 30 min of separation (Fig. 1H). In contrast, in the LTSM test, after 24 hours of separation time, the WT rats had a preference for the novel juvenile, whereas the OXTR $S261A^{+/+}$ rats showed no statistically significant difference (Fig. 1I). We used relative duration of investigation (RDI) = $Time_{novel\ -\ familiar}/Time_{novel\ +\ familiar}$ to compare the retention of social memory. A higher RDI indicates better social memory retention. The LTSM RDI of OXTR $S261A^{+/+}$ rats was significantly lower than that of WT rats (Fig. 1J, left), whereas the RDI of sociability and STSM were not much different (fig. S2A). Heat maps drawn on the basis of the positions of rats represent their typical activity (Fig. 1J, right). These results show that the LTSM of OXTR $S261A^{+/+}$ rats was impaired. We also conducted the object recognition test (ORT) to examine the long-term memory of OXTR $S261A^{+/+}$ rats for objects and found no difference (fig. S2B).

The OXT is known as a profound anxiolytic and antistress factor in the brain (*27*), and the MAPK pathway is critically involved in the regulation of anxiety-like behaviors in the paraventricular nucleus (PVN) (*28*, *29*). We next evaluated the emotional behaviors of OXTR $S261A^{+/+}$ rats using the elevated plus maze (EPM) test, open-field test (OFT), and sucrose preference test. The results suggest increased anxiety-like behaviors without depression of OXTR $S261A^{+/+}$ rats (fig. S2, C to E). Nonetheless, there was no significant correlation between LTSM RDI and anxiety-like behaviors in OXTR $S261A^{+/+}$ rats (fig. S2, F and G).

We used the resident-intruder test paradigm to test the aggressive behaviors of adult male OXTR $S261A^{+/+}$ rats. The OXTR $S261A^{+/+}$ and WT rats showed similar attack latency. Furthermore, the duration of offensive behavior, social behavior and nonsocial exploration, grooming, and inactivity were all statistically analyzed, and no difference was observed (fig. S2H). The olfactory habituation/dishabituation test was used to evaluate the olfactory ability of OXTR $S261A^{+/+}$ rats because social behaviors in rodents are usually based on olfactory signature recognition. Both groups showed similar responses (fig. S2I).

## Different neuronal activity of the medial amygdala is induced by the social interaction of WT and OXTR $S261A^{+/+}$ rats in LTSM

To examine the phosphorylation level of OXTR at $Ser^{261}$ in animals, we customized the p-OXTR $Ser^{261}$ antibody and validated its specificity (fig. S3A). We tested the levels of p-OXTR $Ser^{261}$ and p-ERK1/2 in the prefrontal cortex (PFC), hippocampus (HPC), medial amygdala (MeA), and PVN in both WT and OXTR $S261A^{+/+}$ rats. Western blotting showed the highest level of p-OXTR $Ser^{261}$ in the MeA of WT rats and undetectable levels of p-OXTR $Ser^{261}$ in these regions of OXTR $S261A^{+/+}$ rats. In addition, p-ERK1/2 was lower in OXTR $S261A^{+/+}$ rats than in WT rats (Fig. 2A). On the basis of the above results and other studies linking the MeA and HPC with social memory (*30*–*32*), we tested the level of p-ERK1/2 in the MeA and dorsal and ventral HPC during LTSM test. The level of p-ERK1/2 in the MeA increased after 1 hour of familiarization and, to a much greater extent, after recognition with 24 hours of separation, which is consistent with the expression of c-fos in the MeA during LTSM (*31*). The level of p-ERK1/2 was low in both the dorsal and ventral HPC during LTSM (Fig. 2B).

We hypothesized that the MeA region may play a vital role in impaired LTSM of OXTR $S261A^{+/+}$ rats. To investigate the neuronal activities of the MeA neurons, we used fiber photometry to record real-time $Ca^{2+}$ transients in LTSM of rats (Fig. 2, C and D). The expression of the calcium indicator GCaMP6 and all recording locations were confirmed (Fig. 2E and fig. S3B). The $Ca^{2+}$ changes during the social discrimination test for LTSM were recorded and analyzed (movie S1). The social encounter of WT rats induced a significant $Ca^{2+}$ increase in MeA neurons but relatively lower GCaMP signals during interactions with familiar partners than with novel partners (Fig. 2, F and G). For OXTR $S261A^{+/+}$ rats, the $Ca^{2+}$ increase aligned with social encounters as well (Fig. 2, H and I), whereas no significant difference was observed between familiar and novel interactions (Fig. 2, J and K). The time of LTSM test is shown (Fig. 2L).

The changes of $Ca^{2+}$ signals in MeA during LTSM indicate that MeA neurons are activated when coupled with social interaction. Compared with a great increase to a novel partner, the WT rats had a minor $Ca^{2+}$ signal increase to a familiar one. It may be due to the memory retention of the individual. In contrast, the similar response of OXTR $S261A^{+/+}$ rats to both familiar and novel interactions was consistent with poor social memory maintenance after long-term separation.

## Interference of the phosphorylation of OXTR at $Ser^{261}$ by peptide tat-S261 impairs MeA-mediated LTSM consolidation

We next investigated whether OXTR $Ser^{261}$ phosphorylation in MeA neurons specifically regulates social behaviors. We designed an interfering peptide, tat-S261, which competitively reduces the phosphorylation

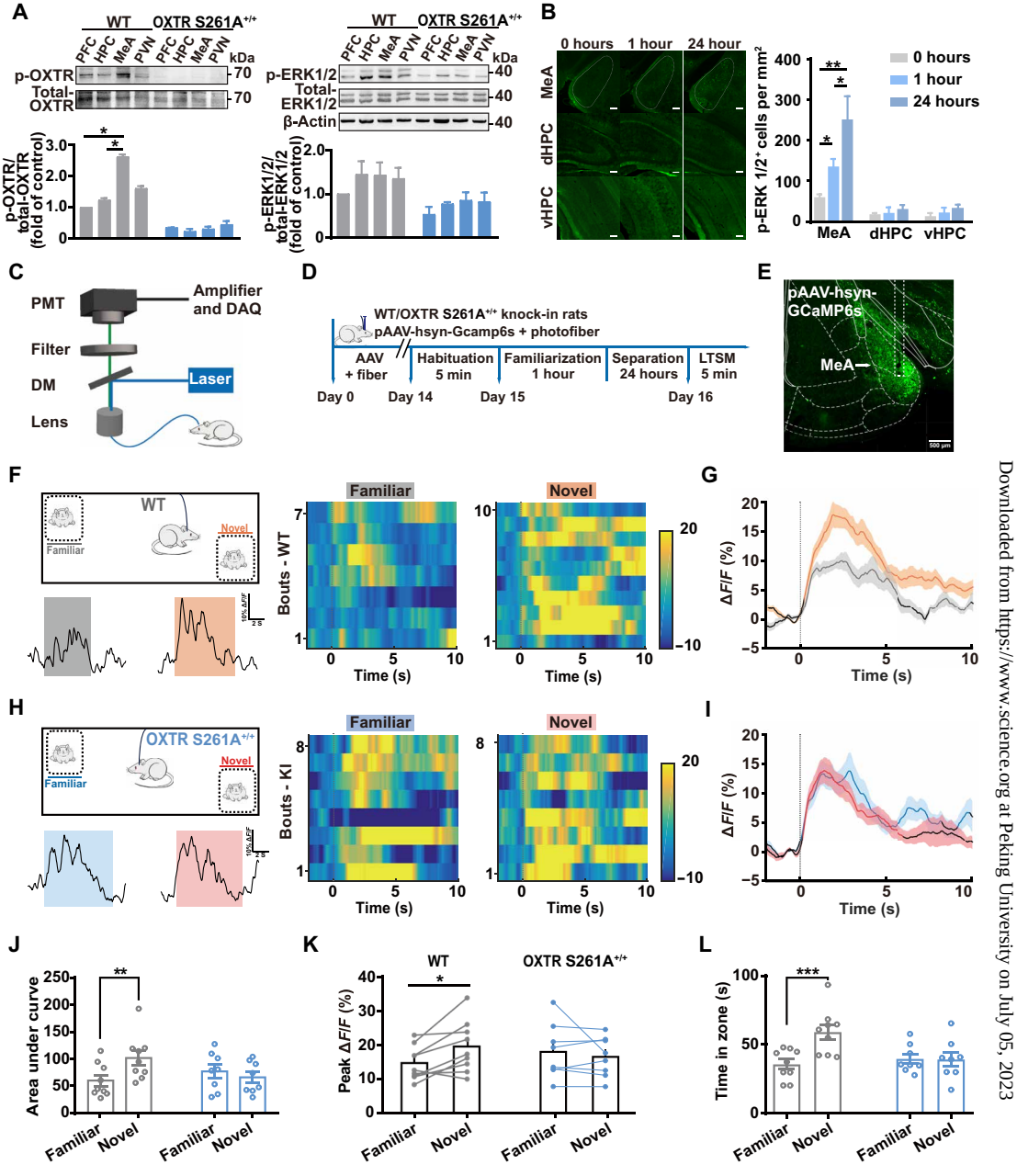


**Fig. 2. Different neuronal activity of MeA is induced by the social interaction of WT and OXTR S261A$^{+/+}$ rats in LTSM.** (**A**) Left: Representative Western blot showing the level of p-OXTR Ser$^{261}$ in different brain regions. Two-way repeated-measures ANOVA, Genotype: $F_{1,4}$ = 460.5, $P$ < 0.0001. Sidak's post hoc test, *$P$ < 0.05. Right: Representative Western blot showing the level of p-ERK1/2 in different brain regions. Two-way repeated-measures ANOVA, Genotype: $F_{1,4}$ = 10.38, $P$ < 0.05. Data are means ± SEM from $n$ = 3 independent experiments. PFC, prefrontal cortex; HPC, hippocampus; MeA, medial amygdala; PVN, paraventricular nucleus. (**B**) Representative and quantification of immunofluorescence images showing p-ERK1/2–positive cells in the MeA during LTSM test. Data are means ± SEM from $n$ = 4 animals. Scale bar, 200 μm. Two-way repeated-measures ANOVA with Sidak's post hoc test, *$P$ < 0.05, **$P$ < 0.01. dHPC, dorsal HPC; vHPC, ventral HPC. (**C**) Schematic diagram of the fiber photometry recording system. DM, dichroic mirror; PMT, photomultiplier tube; DAQ, data acquisition. (**D**) LTSM protocol of WT and OXTR S261A$^{+/+}$ rats during photometry recording. (**E**) Representative coronal section image showing the GCaMP6s-positive neurons in the MeA. Scale bar, 500 μm. (**F**) Left top: Schema of LTSM with photometry. Left bottom: Raw traces of GCaMP from a representative WT rat interacting with familiar (gray) and novel (orange) partners. The colored shading represents occurrences of social encounters. Δ$F$/$F$ represents the change in fluorescence from the mean level before the encounters. Right: Heatmaps illustrating $Ca^{2+}$ signal responses of every bout during 5 min of LTSM testing from a representative WT rat. Color bar, Δ$F$/$F$. (**G**) Average $Ca^{2+}$ signals aligning with the onset of social encounters from all WT rats. The thick lines indicate the means, and the shaded areas indicate the SEM from $n$ = 9 animals. The gray and orange lines represent statistically significant change from baseline (black) during interactions with familiar and novel partners, respectively. Multivariate permutation test, $P$ < 0.05. (**H** and **I**) Same conventions as (F) and (G) but from $n$ = 8 OXTR S261A$^{+/+}$ rats. KI, knock-in. (**J**) The area under the peri-event curve for WT rats (gray) and OXTR S261A$^{+/+}$ rats (blue) from (G) and (I). Data are means ± SEM from $n$ = 9 and 8 animals, respectively. Two-way repeated-measures ANOVA, Genotype × Social stimulus interaction: $F_{1,15}$ = 9.582, $P$ < 0.01. Genotype: $F_{1,15}$ = 0.422, $P$ = 0.526. Social stimulus: $F_{1,15}$ = 3.225, $P$ = 0.093. Sidak's post hoc test, **$P$ < 0.01. (**K**) Magnitudes of peak $Ca^{2+}$ signal changes in WT (gray) and OXTR S261A$^{+/+}$ (blue) MeA neurons. The lines connect the data points from individual rats. Data and $n$ are as in (J). Two-way repeated-measures ANOVA, Genotype × Social stimulus interaction: $F_{1,15}$ = 6.635, $P$ < 0.05. Genotype: $F_{1,15}$ = 0.004, $P$ = 0.948. Social stimulus: $F_{1,15}$ = 1.552, $P$ = 0.232. Sidak's post hoc test, *$P$ < 0.05. (**L**) Total social interaction time by WT (gray) and OXTR S261A$^{+/+}$ rats (blue) during photometry recordings of LTSM. Data and $n$ are as in (J). Two-way repeated-measures ANOVA, Sidak's post hoc test, Genotype × Social stimulus interaction: $F_{1,15}$ = 16.20, $P$ < 0.01. Genotype: $F_{1,15}$ = 1.890, $P$ = 0.189. Social stimulus: $F_{1,15}$ = 15.18, $P$ < 0.01. Sidak's post hoc test, ***$P$ < 0.001.

of OXTR at Ser$^{261}$ by PKD1, and tat-S261A was used as a control (fig. S4, A and B, and details in Materials and Methods).

The peptides were bilaterally injected into the MeA 1 hour before familiarization. As expected, WT rats injected with tat-S261 showed similar performance as OXTR S261A$^{+/+}$ rats in the social discrimination test, specifically in the observation of reduced LTSM, whereas their sociability and STSM profiles were similar to WT rats (Fig. 3, A to C). Compared with the WT rats, the LTSM RDI of tat-S261–injected rats significantly decreased (Fig. 3D), whereas the RDI of sociability and STSM were not much different (fig. S4C).

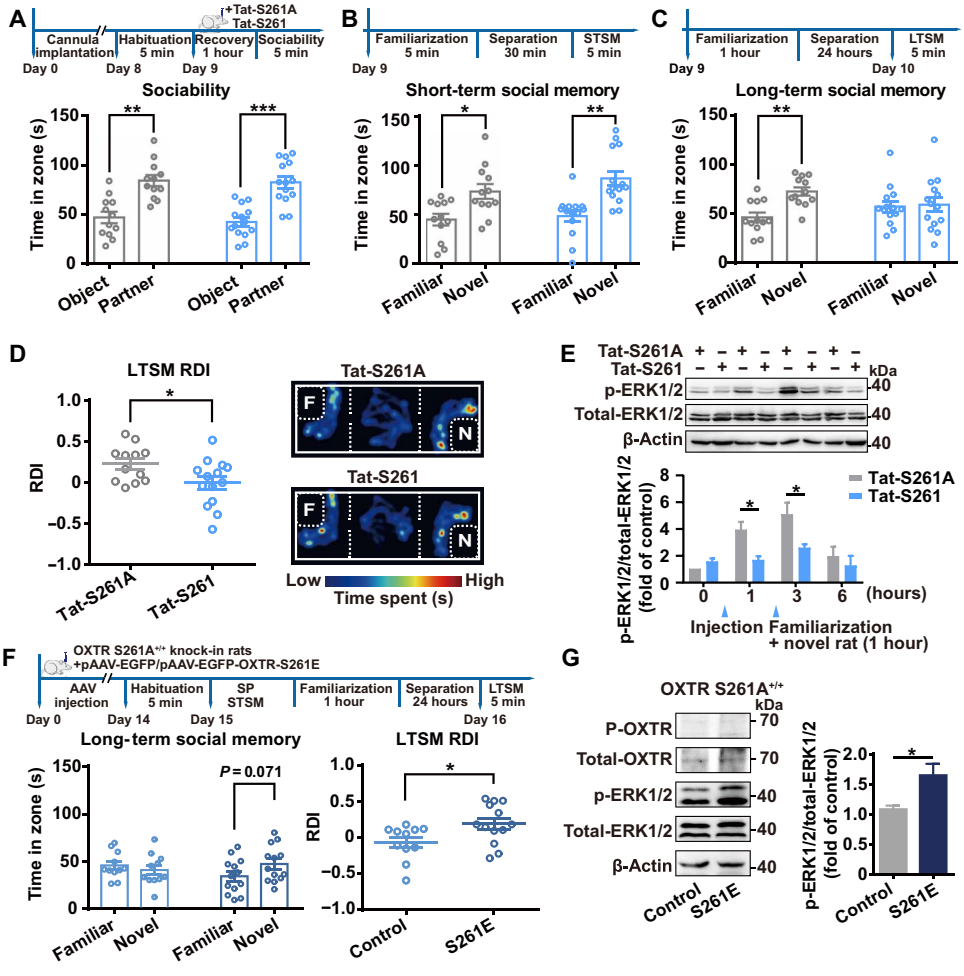


**Fig. 3. Phosphorylation of OXTR at Ser$^{261}$ maintains LTSM through the MeA nucleus.** (**A**) Top: Sociability protocol with interfering peptide injection. Bottom: Time spent by rats injected with tat-S261A (gray, control) and tat-S261 (blue, interfering peptide) in zone around the partner or around the object. Data are means ± SEM from $n = 12$ and 14 animals, respectively. Two-way repeated-measures ANOVA, Peptide × Social stimulus interaction: $F_{1,24} = 0.056$, $P = 0.816$. Peptide: $F_{1,24} = 0.701$, $P = 0.411$. Social stimulus: $F_{1,24} = 35.71$, $P < 0.001$. Sidak's post hoc test, $^{**}P < 0.01$, $^{***}P < 0.001$. (**B**) Top: STSM protocol with interfering peptide injection. Bottom: Time spent by rats injected with tat-S261A (gray, control) and tat-S261 (blue, interfering peptide) in zone around the novel juvenile or around the familiar one. Data and $n$ are as in (A). Two-way repeated-measures ANOVA, Peptide × Social stimulus interaction: $F_{1,24} = 0.397$, $P = 0.534$. Peptide: $F_{1,24} = 2.685$, $P = 0.114$. Social stimulus: $F_{1,24} = 17.3$, $P < 0.001$. Sidak's post hoc test, $^{*}P < 0.05$, $^{**}P < 0.01$. (**C**) Top: LTSM protocol with interfering peptide injection. Bottom: Time spent by rats injected with tat-S261A (gray, control) and tat-S261 (blue, interfering peptide) in zone around the novel juvenile or around the familiar one. Data and $n$ are as in (A). Two-way repeated-measures ANOVA, Peptide × Social stimulus interaction: $F_{1,24} = 3.366$, $P = 0.079$. Peptide: $F_{1,24} = 0.078$, $P = 0.783$. Social stimulus: $F_{1,24} = 4.587$, $P = 0.043$. Sidak's post hoc test, $^{**}P < 0.01$. (**D**) Left: LTSM RDI of rats injected with tat-S261A (gray) or tat-S261 (blue). Data and $n$ are as in (A). Unpaired $t$ test, $^{*}P < 0.05$. Right: Representative heatmaps of the positions of the rats during LTSM testing. (**E**) Representative Western blot showing the level of p-ERK1/2 and total-ERK1/2 with tat-S261A or tat-S261 injection after 1-hour familiarization with a novel juvenile. Data are means ± SEM from $n = 3$ independent experiments. Two-way ANOVA, Genotype × Time: $F_{3,16} = 3.22$, $P = 0.051$. Genotype: $F_{1,16} = 9.449$, $P < 0.01$. Time: $F_{3,16} = 8.613$, $P < 0.01$. Sidak's post hoc test, $^{*}P < 0.05$. (**F**) Top: LTSM protocol with injection of pAAV-EGFP-OXTR-S261E for OXTR S261A$^{+/+}$ rats. Bottom left: Time spent by OXTR S261A$^{+/+}$ rats injected with pAAV-hsyn-EGFP (blue) or pAAV-hsyn-EGFP-OXTR-S261E (dark blue) around the novel juvenile or around the familiar one. Data are means ± SEM from $n = 11$ and 13 animals, respectively. Two-way repeated-measures ANOVA, Virus × Social stimulus interaction: $F_{1,22} = 4.314$, $P = 0.0497$. Virus: $F_{1,22} = 0.196$, $P = 0.662$. Social stimulus: $F_{1,22} = 0.883$, $P = 0.358$. Sidak's post hoc test, S261E Familiar versus Novel: $P = 0.071$. Bottom right: LTSM RDI of rats expressing pAAV-hsyn-EGFP (blue) versus pAAV-hsyn-EGFP-OXTR-S261E (dark blue). Unpaired $t$ test, $^{*}P < 0.05$. (**G**) Representative Western blot showing the expression of p-ERK1/2 and total-ERk1/2 after pAAV-hsyn-EGFP-OXTR-S261E injection in OXTR S261A$^{+/+}$ rats. Data are means ± SEM from $n = 3$ independent experiments. Unpaired $t$ test, $^{*}P < 0.05$.

Furthermore, WT rats with the injection of tat-S261 showed similar $Ca^{2+}$ responses to familiar and novel in the LTSM test as OXTR S261A$^{+/+}$ rats (fig. S4, D and E).

In addition, when the peptides were injected 1 hour before the social discrimination test, the LTSM RDI of both groups was unaffected (fig. S4F), suggesting that memory retrieval was unaffected. We examined the effects of the tat-S261 in vivo through altered p-ERK1/2. Social familiarization was conducted at 1 to 2 hours after the injection, and Western blotting showed that p-ERK1/2 increased within 3 hours and decreased within 6 hours in the control group. In contrast, the tat-S261–injected rats showed lower p-ERK1/2 over time, but p-ERK1/2 increased slightly after social interaction (at 3 hours; Fig. 3E).

Considering that anxiety-like behaviors were observed in OXTR S261A$^{+/+}$ rats, the OFT and EPM were carried out, and no significant difference was found between the WT rats injected with peptides into the MeA (fig. S4, G and H). Therefore, the OXTR phosphorylation status in the MeA region is not related to anxiety-like behaviors. Together, these results suggest that the MeA region plays a critical role in the LTSM consolidation and that blocking the phosphorylation of OXTR at Ser$^{261}$ attenuates the activity of OXTR signaling pathway in the MeA, leading to impaired LTSM.

## Rescue of phosphorylated OXTR in the MeA restores impaired LTSM in OXTR S261A$^{+/+}$ rats

To validate whether MeA neurons and the phosphorylation of OXTR at Ser$^{261}$ are sufficient in LTSM, we injected pAAV-hsyn-EGFP-OXTR-S261E into the MeA region of OXTR S261A$^{+/+}$ rats as a rescue strategy. The expression of virus was confirmed (fig. S5A). Briefly, the OXTR S261A$^{+/+}$ rats expressing S261E showed normal sociability and STSM (fig. S5, B and C). In the LTSM experiment, the OXTR S261A$^{+/+}$ rats injected with pAAV-hsyn-EGFP into the MeA as control showed little discrimination between familiar and novel partners, whereas the OXTR S261A$^{+/+}$ rats expressing S261E showed a mild but not statistically significant preference for novel partners and a significantly higher LTSM RDI compared

with that of the controls (Fig. 3F). We also found an increase of p-ERK1/2 in the MeA of rescued OXTR S261A$^{+/+}$ rats (Fig. 3G).

The anxiety-like behaviors of rescued OXTR S261A$^{+/+}$ rats were tested afterward. No significant improvement in performance in the EPM or OFT was observed in the rescued group (fig. S5, D and E). Together, the expression of OXTR-S261E in OXTR S261A$^{+/+}$ rats restored social memory persistence after long-term separation, and the phosphorylation of OXTR at Ser$^{261}$ in the MeA is necessary and sufficient for LTSM.

## Conditional knockout of PKD1 in the MeA leads to impaired LTSM in mice

Thus far, our results have demonstrated that the phosphorylation of OXTR at Ser$^{261}$ regulates LTSM in MeA neurons. To examine the functions of PKD1 in this process, and because we were technically unable to locally manipulate *Pkd1* expression in rats, we injected pAAV-hsyn-Cre virus into the MeA of *Pkd1*$^{fl/fl}$ mice. Virus expression was confirmed, and a decreased abundance of PKD1, p-Ser$^{261}$ OXTR, and p-ERK1/2 was detected (Fig. 4, A and B). No significant difference in sociability and STSM was observed compared to control mice (Fig. 4, C and D, and fig. S5F). However, the results of LTSM in mice were not consistent with that of rats, in that social memory after 24 hours of separation was barely detectable. We then plotted the kinetics of the social memory RDI and found that the retention of social memory declined over time, and preference tended to vanish after 24 hours of separation (Fig. 4E, bottom left). Therefore, LTSM was tested in control and *Pkd1*$^{fl/fl}$ mice expressing Cre in the MeA after 2, 6, 12, and 24 hours of separation. A significant difference of RDI was observed at 6 and 12 hours of separation (Fig. 4, E to G). Collectively, therefore, ablation of PKD1 in the MeA resulted in decreased social memory maintenance as well, supporting its functional role in OXTR-mediated signaling. We note, however, that we cannot extrapolate these results in mice directly to rats in which OXTR was manipulated.

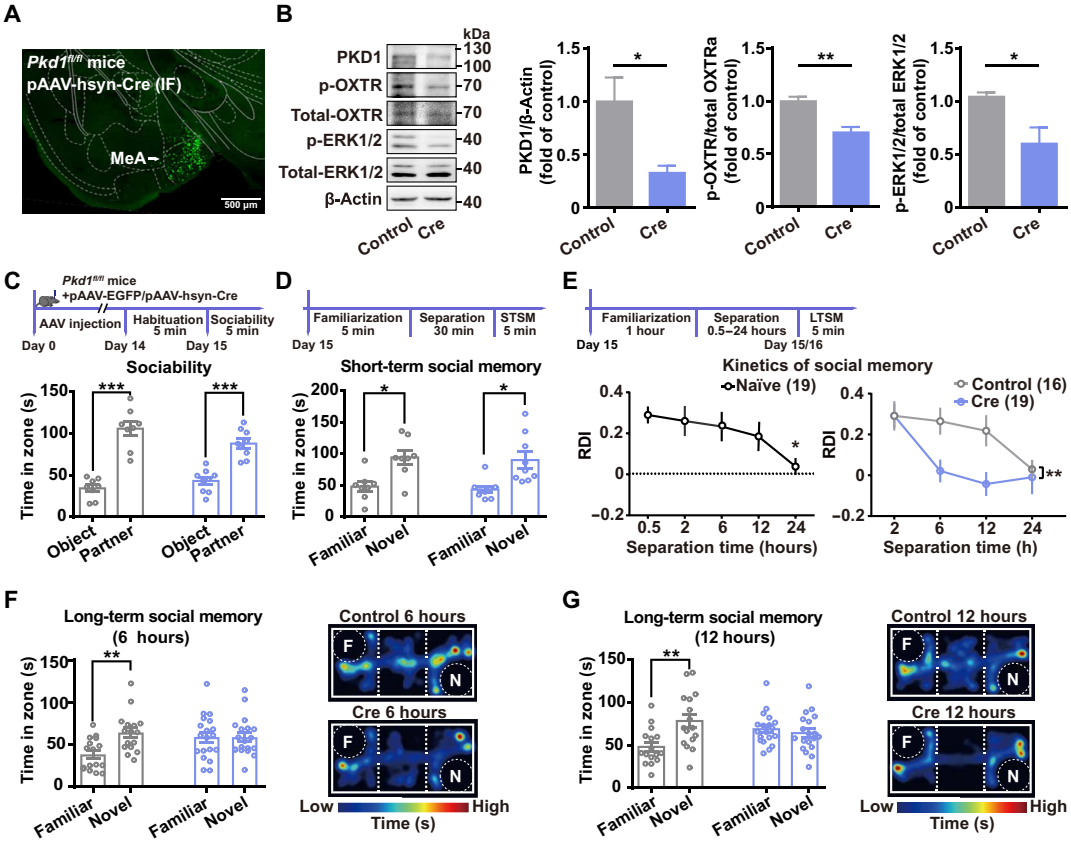


**Fig. 4. Conditional knockout of PKD1 in MeA leads to impaired LTSM.** (**A**) Representative coronal section and immunofluorescence (IF) staining of Cre recombinase image showing the pAAV-hsyn-Cre–positive cells in the MeA of *Pkd1*$^{fl/fl}$ mice. Scale bar, 500 μm. (**B**) Representative Western blot showing the levels of PKD1, p-OXTR Ser$^{261}$, and p-ERK1/2 after pAAV-hsyn-EGFP or pAAV-hsyn-Cre injection in the MeA region of *Pkd1*$^{fl/fl}$ mice. Data are means ± SEM from $n = 3$ independent experiments. Unpaired *t* test, $^{*}P < 0.05$, $^{**}P < 0.01$. (**C**) Top: Sociability protocol with *Pkd1*$^{fl/fl}$ mice. Bottom: Time spent of *Pkd1*$^{fl/fl}$ mice (gray) and *Pkd1*$^{fl/fl}$ mice expressing Cre in the MeA (blue) in zone around the partner or around the object. Data are means ± SEM from $n = 8$ and 9 animals, respectively. Two-way repeated-measures ANOVA, Virus × Social stimulus interaction: $F_{1,15} = 5.034$, $P < 0.05$. Virus: $F_{1,15} = 0.602$, $P = 0.45$. Social stimulus: $F_{1,15} = 95.08$, $P < 0.001$. Sidak's post hoc test, $^{***}P < 0.001$. AAV, adeno-associated virus. (**D**) Top: STSM protocol with *Pkd1*$^{fl/fl}$ mice. Bottom: Time spent by *Pkd1*$^{fl/fl}$ mice (gray) and *Pkd1*$^{fl/fl}$ mice expressing Cre in the MeA (blue) in zone around the novel juvenile or around the familiar one. Data and *n* are as in (C). Two-way repeated-measures ANOVA, Virus × Social stimulus interaction: $F_{1,15} = 0.0005$, $P = 0.983$. Virus: $F_{1,15} = 0.402$, $P = 0.536$. Social stimulus: $F_{1,15} = 15.41$, $P < 0.01$. Sidak's post hoc test, $^{*}P < 0.05$. (**E**) Top: LTSM protocol with *Pkd1*$^{fl/fl}$ mice. Bottom left: The LTSM RDI of naïve WT mice (black) with separation times of 0.5, 2, 6, 12, and 24 hours. One-way repeated-measures ANOVA with Tukey's post hoc test, 0.5 hours versus 24 hours, $^{*}P < 0.05$. Data are means ± SEM from $n = 19$ animals. Bottom right: The LTSM RDI of control (gray) and Cre (blue) with separation times of 2, 6, 12, and 24 hours. Data are means ± SEM from $n = 16$ and 19 animals, respectively. Two-way repeated-measures ANOVA, Virus × Separation time interaction: $F_{3,99} = 1.992$, $P = 0.120$. Virus: $F_{3,99} = 6.142$, $P < 0.001$. Separation time: $F_{3,99} = 10.11$, $P < 0.01$. Sidak's post hoc test, $^{**}P < 0.01$. (**F**) Left: Time spent by *Pkd1*$^{fl/fl}$ mice (gray) and *Pkd1*$^{fl/fl}$ mice expressing Cre in the MeA (blue) in zone around the novel juvenile or around the familiar one after 6 hours of separation. Data are means ± SEM from $n = 16$ and 19 animals, respectively. Two-way repeated-measures ANOVA, Virus × Social stimulus interaction: $F_{1,33} = 7.103$, $P < 0.05$. Virus: $F_{1,33} = 1.524$, $P = 0.226$. Social stimulus: $F_{1,33} = 7.03$, $P < 0.05$. Sidak's post hoc test, $^{**}P < 0.01$. Right: Representative heatmaps of the LTSM tests after 6 hours of separation. (**G**) Same convention as (F) but after 12 hours of separation. Two-way repeated-measures ANOVA, Virus × Social stimulus interaction: $F_{1,33} = 7.206$, $P < 0.05$. Virus: $F_{1,33} = 0.453$, $P = 0.506$. Social stimulus: $F_{1,33} = 3.912$, $P = 0.056$. Sidak's post hoc test, $^{**}P < 0.01$.

### OXTR-$G_q$ coupling and the phosphorylation of PKD1 are increased by OXTR phosphorylation, forming a positive feedback loop

The results thus far led us to explore the cellular mechanism underlying the phosphorylation of OXTR by PKD1 in social memory. It has been reported that the IL3 and C terminus of OXTR are domains involved in coupling to the $G_q$ protein (*33*). Hence, we examined the binding between $G_{q/11}$ and OXTR in different OXTR phosphorylation status. Coimmunoprecipitation experiments showed that OXTR-$G_q$ coupling was enhanced by PKD1 overexpression whereas decreased with myc-his-DNPKD1 overexpression after OXT stimulation (Fig. 5, A and B). A similar strategy was used to assess the consequences of OXTR S261A and S261E mutations. OXTR S261A reduced the binding of OXTR and $G_q$, whereas OXTR S261E showed the opposite effect (Fig. 5, C and D). Thus, the phosphorylation of OXTR at $Ser^{261}$ by PKD1 affects the OXTR-$G_q$ binding and downstream signaling, including the activation of the MAPK cascade.

Multiple hormones, growth factors, and neurotransmitters activate PKD1 downstream of the GPCR signaling, especially by a protein kinase C (PKC)–dependent pathway (*34*). We examined whether the activity of PKD1 itself is altered during OXTR signaling activation. Unexpectedly, the phosphorylation of PKD1 at $Ser^{744/748}$ (*35*) was markedly increased after OXT stimulation (Fig. 5E). Application of the PKC inhibitor GF109203X effectively inhibited OXT-induced phosphorylation of PKD1 at $Ser^{744/748}$ and of ERK1/2 (Fig. 5F), whereas the basal levels of both phosphorylated proteins were unchanged (fig. S6A). Given that the phosphorylation of PKD1 at $Ser^{744/748}$ reportedly stabilizes the enzyme in an active conformation

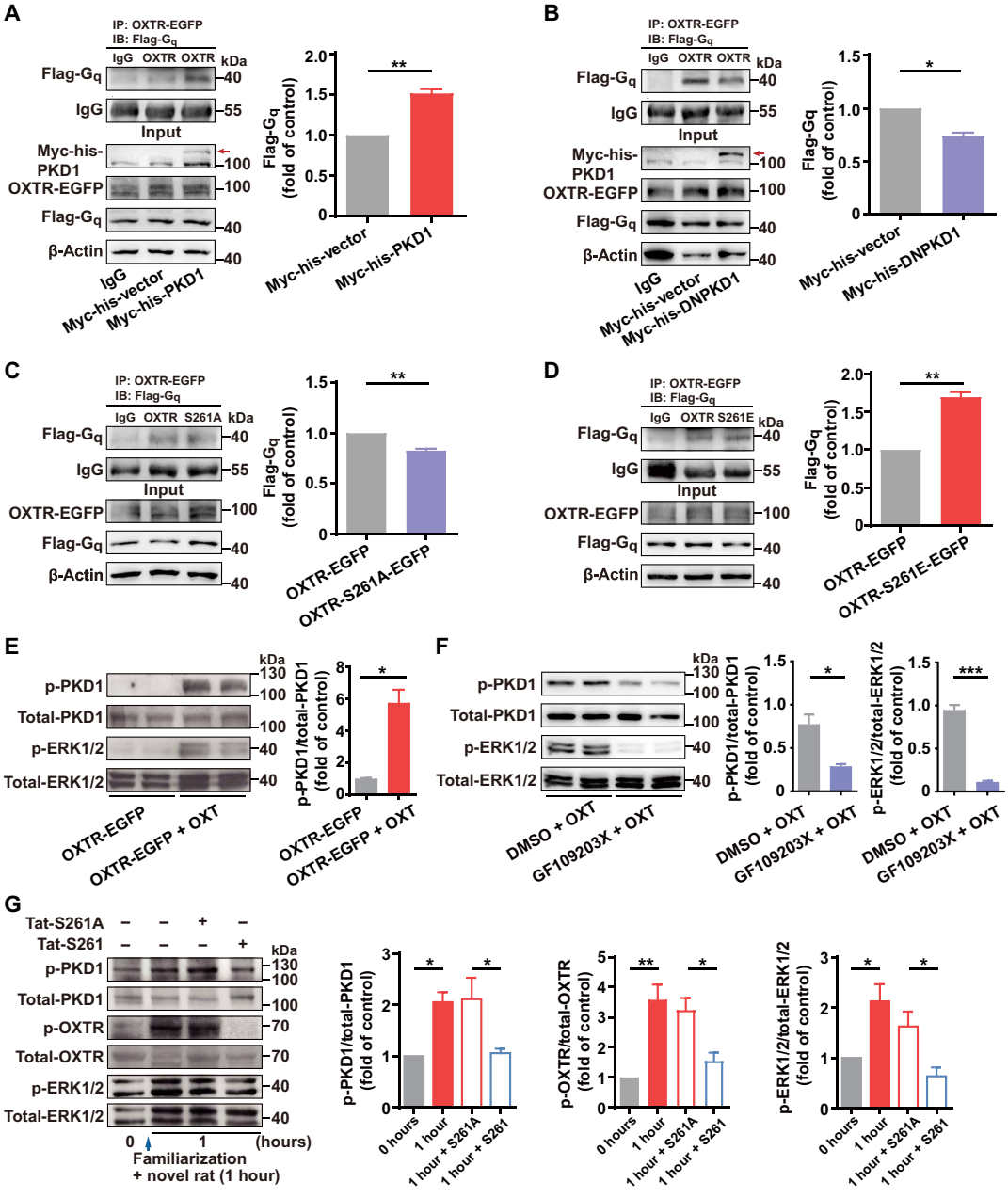


**Fig. 5. OXTR-$G_q$ coupling and the phosphorylation of PKD1 are modulated by the phosphorylation of OXTR at $Ser^{261}$.** (**A** and **B**) Representative immunoblot (IB) of $G_q$ coimmunoprecipitated with OXTR (IP) in HEK293 cells transfected with myc-his-vector, myc-his-PKD1, myc-his-DNPKD1, OXTR-EGFP, and Flag-$G_q$ with OXT treatment. (**C** and **D**) Representative immunoblots (IB) of $G_q$ coimmunoprecipitated with OXTR (IP) in HEK293 cells transfected with myc-his-PKD1, OXTR-EGFP, OXTR-EGFP-S261A, OXTR-EGFP-S261E, and Flag-$G_q$ with OXT treatment. (**E**) Representative Western blot of the phosphorylated PKD1 (p-PKD1 $Ser^{744/748}$), total-PKD1, p-ERK1/2, and total-ERK1/2 in HEK293 cells transfected with myc-his-PKD1and OXTR-EGFP with or without OXT treatment. (**F**) Representative Western blot of the phosphorylated PKD1 (p-PKD1 $Ser^{744/748}$), total-PKD1, p-ERK1/2, and total-ERK1/2 in HEK293 cells transfected with myc-his-PKD1 and OXTR-EGFP with OXT treatment after 1 hour of incubation with PKC inhibitor GF109203X (1 nM) or DMSO. For (A) to (F), data are means ± SEM from $n = 3$ independent experiments; unpaired $t$ test or unpaired $t$ test with Welch's correction: $^*P < 0.05$, $^{**}P < 0.01$, $^{***}P < 0.001$. (**G**) Representative Western blot showing the levels of p-PKD1, p-OXTR $Ser^{261}$, and p-ERK1/2 in the MeA after 1 hour of familiarization (0 hours versus 1 hour, lanes 1 and 2) and after tat-S261 injection (tat-S261A versus tat-S261, lanes 3 and 4). Data are means ± SEM from $n = 4$ independent experiments. One-way ANOVA with Tukey's post hoc test, $^*P < 0.05$, $^{**}P < 0.01$.

(*36*) and the results above that PKD1 promotes the OXTR signaling (Figs. 1C and 5A), we speculated that the phosphorylation of OXTR and PKD1 form a feed-forward regulation loop. Thus, we examined the phosphorylation levels of PKD1, OXTR, and ERK1/2 in the MeA of naïve rats and rats injected with tat-S261. Increased p-PKD1 Ser$^{744/748}$, p-OXTR Ser$^{261}$, and p-ERK1/2 were observed after 1 hour of social interaction, whereas the phosphorylations were suppressed by tat-S261 (Fig. 5G). These results suggest a positive feedback mechanism by which the activated OXTR promotes the activation of PKD1, which in turn increases the p-OXTR Ser$^{261}$ and triggers enhanced OXTR-$G_q$ binding and downstream activation.

### *OXTR* single-nucleotide polymorphism rs200362197 blocks the phosphorylation of OXTR at Ser$^{261}$ and attenuates downstream signaling of the OXTR pathway

We further investigated the possible function of the phosphorylation of OXTR at Ser$^{261}$ in humans and found that the *OXTR* single-nucleotide polymorphism (SNP) rs200362197 (https://www.ncbi.nlm.nih.gov/snp/rs200362197) is located in the conserved recognition region of the PKD1 phosphorylation site of OXTR. The SNP causes a missense mutation in which arginine is mutated to histidine (R258H; Fig. 6A). We hypothesized that the SNP impairs the function of OXTR similar to the S261A and specifically developed an R258H mutation in the rat GST-OXTR-IL3 plasmid. Kinase assays showed little phosphorylation of GST-OXTR-IL3 R259H (Fig. 6B). The level of p-ERK1/2 was lower in the presence of the SNP after OXT stimulation and was not significantly altered under basal conditions, as expected (Fig. 6C and fig. S6B). The coupling of OXTR and $G_q$ in the presence of the SNP decreased as well (Fig. 6D). Last, the p-PKD1 decreased with SNP expression after OXT stimulation (Fig. 6E). Together, the results suggested that the SNP mutation attenuates OXTR downstream signaling and that rs200362197 may cause defects in OXTR function.

## DISCUSSION

Despite a sizeable body of research that has examined the function of OXT and its receptor OXTR by antagonists or genetic knockout,

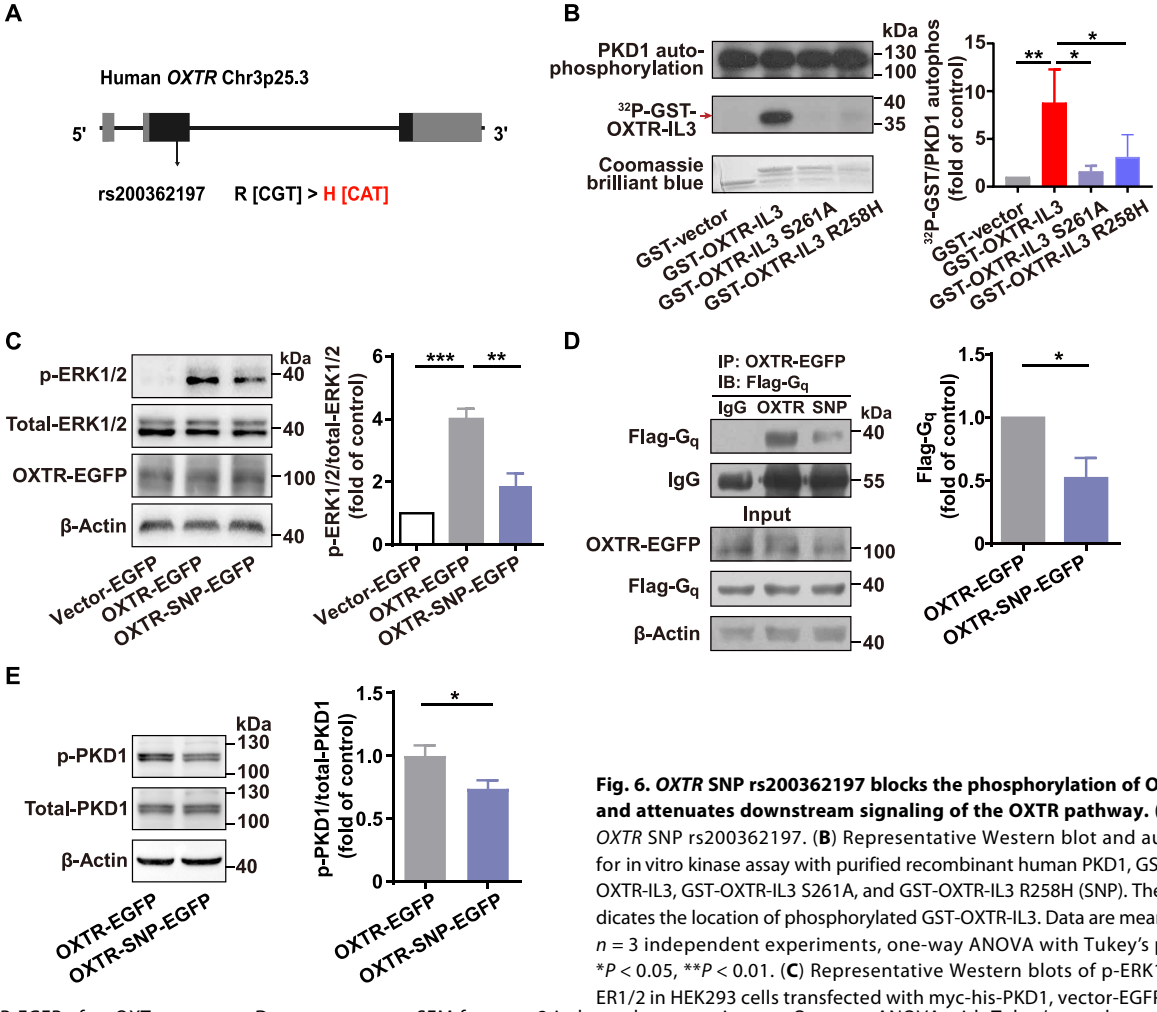


**Fig. 6. *OXTR* SNP rs200362197 blocks the phosphorylation of OXTR at Ser$^{261}$ and attenuates downstream signaling of the OXTR pathway.** (**A**) Schema of *OXTR* SNP rs200362197. (**B**) Representative Western blot and autoradiogram for in vitro kinase assay with purified recombinant human PKD1, GST-vector, GST-OXTR-IL3, GST-OXTR-IL3 S261A, and GST-OXTR-IL3 R258H (SNP). The red arrow indicates the location of phosphorylated GST-OXTR-IL3. Data are means ± SEM from $n = 3$ independent experiments, one-way ANOVA with Tukey's post hoc test, $^*P < 0.05$, $^{**}P < 0.01$. (**C**) Representative Western blots of p-ERK1/2 and total-ER1/2 in HEK293 cells transfected with myc-his-PKD1, vector-EGFP, OXTR-EGFP, and OXTR-SNP-EGFP after OXT treatment. Data are means ± SEM from $n = 3$ independent experiments. One-way ANOVA with Tukey's post hoc test, $^{**}P < 0.01$, $^{***}P < 0.001$. (**D**) Representative immunoblots (IB) of $G_q$ coimmunoprecipitated with OXTR (IP) in HEK293 cells transfected with myc-his-PKD1, OXTR-EGFP, OXTR-SNP-EGFP, and Flag-$G_q$ after OXT treatment. Data are means ± SEM from $n = 3$ independent experiments. Unpaired *t* test with Welch's correction, $^*P < 0.05$. (**E**) Representative Western blot of the phosphorylated PKD1 (p-PKD1 Ser$^{744/748}$) and total-PKD1 in HEK293 cells transfected with myc-his-PKD1, OXTR-EGFP, and OXTR-SNP-EGFP after OXT treatment. Data are means ± SEM from $n = 4$ independent experiments. Unpaired *t* test, $^*P < 0.05$.

the specific signaling pathway(s) regulating and regulated by the OXTR in social memory are not yet well understood. Here, we demonstrate that the phosphorylation of OXTR at $Ser^{261}$ by PKD1 is vital in the function of OXTR signaling in the MeA in rodents. Specifically, once the OXTR is activated by extracellular OXT, which occurs during social interaction (*37*), the activity of PKD1 is up-regulated through a PKC-dependent pathway. Activated PKD1 then phosphorylates the OXTR and enhances OXTR-$G_q$ coupling, which leads to increased p-ERK1/2. Therefore, a positive feedback loop is formed that amplifies signals to promote the OXTR pathway (Fig. 7). Increasingly, posttranslational modifications in the regulation and pharmacology of GPCRs in relationship to biased agonism have been established (*38*, *39*). Studies show that the OXTR has two or three potential glycosylation sites in its extracellular N-terminal domain that are not essential for its activity (*40*). The cysteine residues as palmitoylation sites in extracellular loops and the C terminus of the OXTR fail to produce significant functional alterations (*41*). Rapid and transient phosphorylation of OXTR C terminus by GPCR kinases and PKC initiates β-arrestin–mediated OXTR desensitization (*10*, *42*, *43*). Our study reveals a functional posttranslational modification that phosphorylation in the IL3 of OXTR at $Ser^{261}$ increases the activity of the OXTR signaling after OXT stimulation. The phosphorylation of the OXTR at $Ser^{261}$ is abolished in OXTR $S261A^{+/+}$ rats, leading to impaired LTSM. These results are direct evidence that phosphorylation of OXTR promotes the functions of the OXT system and associated social behavior mediated by MeA neurons.

Different brain regions and brain circuits have been studied in social memory (*44*–*49*). A DG-CA2/CA3 axis of OXTR-expressing cells in the HPC has been described in discrimination of social stimuli, and conditional deletion of OXTR in CA2/CA3a impairs the persistence of long-term social recognition memory in mice (*7*, *50*). Rodents mainly rely on olfactory signatures to communicate social status, and the principal neurons in the MeA process main and accessory olfactory inputs to achieve information convergence, thus modulating social recognition and memory (*51*–*53*). Therefore, it is understandable that the HPC acts as a hub to summarize episodic memory and responses to both social and nonsocial information (*4*, *54*), whereas the MeA plays a pivotal role in LTSM and undergoes long-term depression in an OXT-dependent manner (*30*). *Oxt* knockout mice fail to display social recognition, and these deficits can be rescued by OXTR activation in the MeA (*32*). MeA neurons also represent different social information during social encounters (*55*). Our results also show that the phosphorylation-dependent modulation of OXTR and ERK1/2 are related to the MeA during LTSM, demonstrating the specific regulation of social memory mediated by MeA. One of the major differences between long-term and short-term memory (social and nonsocial) is the consolidation process that is the result of protein synthesis (*56*, *57*). Long-lasting social memory requires protein synthesis at a long range of time scales after social interaction (*58*, *59*). In our study described here, animals exhibited an unaffected learning process and memory retrieval ability, whereas an enhanced LTSM was accompanied by an increased abundance of p-ERK1/2 in the MeA. Because the activation of p-ERK1/2 is vital to MAPK signaling cascades downstream of the OXTR and is critical for protein synthesis, we speculate that the phosphorylation of OXTR $Ser^{261}$ by PKD1 after social interaction may lead to protein synthesis and the consolidation of long-term memory.

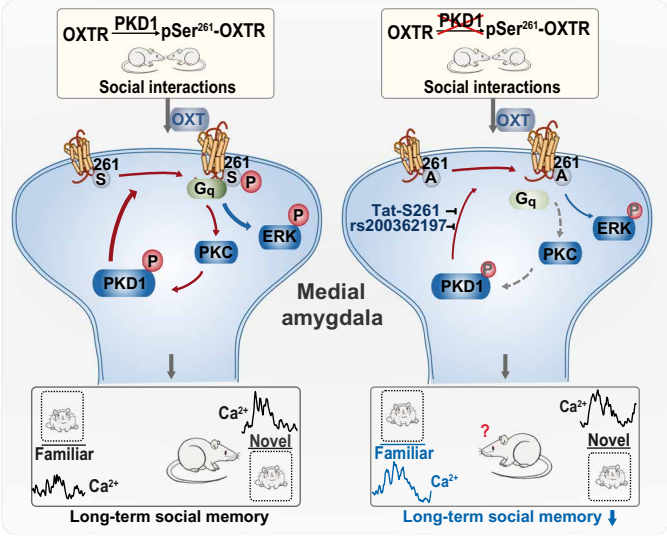


**Fig. 7. Model of the mechanism.** Working model of the phosphorylation-dependent positive feedback loop of the OXTR and PKD1 and its effects on the MeA-mediated LTSM consolidation.

Unexpectedly, we found that the positive feedback of OXTR and PKD1 is important for OXTR signaling. Positive feedback regulation amplifies input signals, thereby providing enhanced system sensitivity (*60*). In our study, this positive feedback in the MeA amplified OXTR signaling activity involved in the MAPK cascade after OXT application or social stimulation, leading to LTSM consolidation. Despite numerous studies that have uncovered connections between the OXT system and various social behaviors, few studies have reported *OXTR* deletions in disease. In contrast, the association of SNPs in *OXTR* with autism spectrum disorder is more commonly observed (*61*). Accordingly, removing the receptor from the whole or part of the brain to study the OXT system is more specific for functional research but is less relevant to the disease. In our study, the extensive deactivation of the OXTR signaling pathway by mutagenesis impairs specific behaviors, indicating that the OXTR $S261A^{+/+}$ knock-in rats could be a model for studying the weakened OXT system. We also identified that the *OXTR* SNP rs200362197 is located in the conserved recognition region of the PKD1 phosphorylation site of OXTR and attenuates downstream of the OXTR signaling, similar to the OXTR S261A. These results indicate the possible impacts and mechanism of single-nucleotide mutations on social behaviors. The clinical information about the mutation is still inadequate, and more data are needed to analyze the clinical phenotypes in future studies.

Studies on the *OXTR* gene have revealed several SNP loci that are strongly associated with the phenotypes of many disorders, including autism spectrum, schizophrenia, and those related to anxiety (*2*, *62*, *63*). Polymorphisms in the *OXTR* gene also affect functional connectivity in the human brain and affect the social behavior of both humans and animals after nasal application of OXT (*64*–*66*). Considering the contradictory results of long-term OXT treatment in clinical trials (*67*–*69*), further investigation on the regulation and modification of OXTR is of urgent need.

In summary, our research elucidates the mechanism of the posttranslational phosphorylation of OXTR at $Ser^{261}$ and a positive feedback regulation between OXTR and PKD1, which amplifies OXTR signaling and contributes to LTSM consolidation in the MeA. These results provide brain area– and cellular signaling–specific evidence

for social memory regulation by the modification of OXTR and insights into the molecular mechanisms underlying social deficits. Moreover, we have revealed the fine-tuned and specific functions of OXTR signaling, and these findings may be helpful in identifying more efficient therapeutic strategies to applicate the OXT system and to improve social learning and prosocial behaviors.

## MATERIALS AND METHODS

### Animals

Animal care and use strictly followed institutional guidelines and governmental regulations. All experiments were performed according to the guidelines of the Animal Care and Use Committee of Peking University Health Science Center.

The animals used in the experiments were male Sprague-Dawley rats and OXTR S261A$^{+/+}$ knock-in rats (8 to 12 weeks for adults; Cyagen Biosciences Inc., China), male Wistar rats (4 to 5 weeks for juveniles and 9 weeks for adults), C57BL/6J mice, and *PKD1*$^{fl/fl}$ mice (3 weeks for juveniles and 6 to 10 weeks for adults; Cyagen Biosciences Inc.). See table S1 for ages of animals used in experiments. Rats were housed in groups of three, and mice were housed in groups of six to avoid social isolation except for special experimental conditions in a temperature-controlled (23° ± 2°C) and humidity-controlled (50 ± 5%) environment. The animals were maintained on a 12-hour light/dark cycle with ad libitum access to food and water, and all behavioral procedures were performed during the dark cycle. The littermates of the male animals were randomly assigned to experimental groups. All animals were handled 3 to 7 days before the behavior tests.

### Cells

HEK293A cells were maintained in Dulbecco's modified Eagle's medium plus 10% fetal bovine serum (Hyclone) at 37°C in 5% $CO_2$. Chemicals used for cell experiments are OXT [diluted to 5 mM by phosphate-buffered saline (PBS) and stored at −20°C; catalog no. 1491300, Sigma-Aldrich] and GF109203X [diluted to 1 mM by dimethyl sulfoxide (DMSO) and stored at −20°C; catalog no. S7208, Selleck]. For OXT treatment assays, cells were treated with 50 nM OXT for 5 min, except in fig. S1C where different treatment durations were tested.

### Plasmid construction, mutation, and transfection

The construct in which GST was fused with IL3 and C terminus of the OXTR (GST-OXTR-IL3/C-terminal) was generated and subcloned into an EGFP-N1 plasmid. The myc-his-PKD1 construct was generated and subcloned into a pcDNA 3.1/myc-His C plasmid. The Flag-$G_q$ construct was generated from the rat brain and subcloned into a FLAG-pCMV-Tag 2 plasmid.

Mutants of OXTR-IL3 (S261A, S261E, and R258H) and myc-his-DNPKD1 (D727A) were created with the QuickChange site-directed mutagenesis kit (Stratagene). All constructs were confirmed by DNA sequencing (Ruibiotech).

The transfection of HEK293A cells was performed with Lipofectamine 2000/3000 (Invitrogen). Cells were used 24 to 36 hours after transfection.

### In vitro kinase assay

The in vitro kinase assay was conducted as previously described (*25*). Briefly, 20 ng of active PKD1 (Upstate Biotechnology) was resuspended in assay buffer to a volume of 25 ml at a final concentration of 0.8 ng/ml. To initiate the reaction, 10 ml of the phosphorylation mixture (assay buffer containing 5 μCi [γ-$^{32}$P] adenosine triphosphate and one of the following GST fusion proteins: GST-vector, GST-OXTR-C-terminal, GST-OXTR-IL3, GST-OXTR-IL3 S261A, or GST-OXTR-SNP) was added. The mixture was incubated at 30°C for 30 min, and the reaction was terminated by the addition of SDS–polyacrylamide gel electrophoresis (SDS-PAGE) sample buffer. After boiling for 5 min, the samples were subjected to SDS-PAGE. The gels were stained with Coomassie brilliant blue, dried, and exposed to x-ray film for autoradiography.

### Pull-down assay

GST-fusion proteins were expressed in *Escherichia coli* BL21 (DE3) cells and purified using Glutathione Sepharose 4 Fast Flow (Amersham Pharmacia) according to the manufacturer's instructions. His6-fusion proteins were purified using Ni–nitrilotriacetic acid agarose beads (QIAGEN) following the manufacturer's instructions. For binding assays, eluted His6-fusion protein was incubated with immobilized GST (as a control) or with GST-fusion protein for 2 hours at 4°C. The mixture was then washed, eluted, and subjected to Western blot analysis.

### Coimmunoprecipitation

Protein extracts from transfected cells or brain tissues were prepared for Western blots. Extracts containing 400 to 500 μg of protein were incubated with antibodies against GFP (1:50) and protein A–Sepharose CL-4B resin (GE Healthcare) at 4°C overnight. The immunoprecipitates were washed six times with 0.1% Triton X-100 in tris-buffered saline (TBS). The final pellets were boiled in SDS-PAGE sample buffer and subjected to Western blot analysis.

### Western blot analysis and antibodies

Brain tissues and transfected cells were homogenized in ice-cold lysis buffer and rotated at 4°C for 1 hour. The supernatant was extracted by centrifugation at 12,000 rpm and 4°C for 5 min. Equal amounts of protein extracts were denatured, subjected to SDS-PAGE (10%), and transferred onto nitrocellulose membranes. The membranes were blocked with 5% nonfat milk in TBS with Tween 20 (TBST) for 1 hour at room temperature and incubated with the appropriate primary antibody overnight at 4°C: p-PKD1 S744/748 (catalog no. 2054, Cell Signaling Technology), PKD1 (catalog no. sc-639, Santa Cruz Biotechnology), p-OXTR Ser$^{261}$ (customized by MBL Beijing Biotech, polyclonal antibody from rabbit), GFP (catalog no. sc-8334, Santa Cruz Biotechnology), p-ERK1/2 (catalog no. 4370, Cell Signaling Technology), ERK (catalog no. sc-93, Santa Cruz Biotechnology), β-actin (catalog no. TA-09, ZSGB-Bio), Myc (catalog no. WH0004609M2, Sigma-Aldrich), and Flag (catalog no. F3165, Sigma-Aldrich) (1:1000); and OXTR [catalog no. sc-8102, Santa Cruz Biotechnology (discontinued) and catalog no. NBP1-28487, Novus, USA. The two antibodies showed similar results, 1:200 to 1:500]. After washing three times with TBST, the membranes were incubated with secondary antibody for 1 hour at room temperature, washed again, and lastly developed with a Lightning chemiluminescence kit.

A Western blot to examine the specificity of the antibody for p-OXTR Ser$^{261}$ in HEK293A cells is shown in fig. S3A. The dephosphorylation of proteins was done by alkaline phosphatase (catalog no. EF0651, Thermo Fisher Scientific).

### Peptide

The interfering peptide contained a tat sequence (a peptide consisting of 9 amino acids that can transport proteins across the cell membrane) and 14 amino acids around the rat OXTR $Ser^{261}$ site to form a 24–amino acid interfering peptide, tat-OXTR-IL3-S261 (RKKRRQRRR-AALARVS**S**VKLISKA). A similar fusion peptide with the tat sequence and the OXTR S261A mutation, tat-OXTR-IL3-S261A (RKKRRQRRR-AALARVS**A**VKLISKA), was used as a control.

Tat-OXTR-IL3-S261 and Tat-OXTR-IL3-S261A were synthesized and purified by GL Biochem. The mass and purity of the peptides were verified by high-performance liquid chromatography. The injection dose is 20 μg/μl and 0.5-μl volume each side for rats.

### Fluorescent immunostaining

Rats or mice were anesthetized with 10% chloral hydrate and briefly perfused transcardially with saline within 15 min, followed by paraformaldehyde in 4% immediately. Then, the isolated brains were postfixed overnight and cryoprotected in 20 and 30% sucrose in 0.1 M PBS. Coronal sections (30 μm thick) were cut with a cryostat (CM3050S, Leica). The sections were washed three times with PBS for 5 min each before being blocked with a 3% bovine serum albumin solution (0.3% Triton X-100, 0.1 M PBS) for 40 min at room temperature. The sections were then incubated with antibody p-ERK1/2 (catalog 4370, Cell Signaling Technology) and Cre recombinase (catalog no. 15036, Cell Signaling Technology) (1:1000) for 24 hours at 4°C. After incubation, the sections were washed three times and then incubated at 4°C overnight with secondary antibodies. Last, the sections were washed three times and air-dried before being placed on coverslips with mounting medium. Images were acquired by an Olympus whole slide scanner VS120-S6-W.

### Stereotaxic surgery

Rats or mice were anesthetized with sodium pentobarbital (rats, 1%; mice, 0.05%) and placed on a stereotaxic apparatus (RWD Life Technology). The scalp was incised to expose the skull after the hair was shaved, and the incision site was cleaned with iodine and medical alcohol. The connective tissue was gently removed from the skull surface with cotton swabs. Then, small craniotomy holes were drilled. The virus was injected by a Nanoliter 2000 microprocessor controller (World Precision Instruments Inc.) via a glass electrode at 60 nl/min, and the electrode was left in place for an additional 5 min.

pAAV-hsyn-GCaMP6s [serotype 2/9, titer $4.35 \times 10^{12}$ viral genomes (v.g.)/ml; BrainVTA], pAAV- hsyn-EGFP-OXTR-S261E (serotype 2/9, titer $6.25 \times 10^{12}$ v.g./ml; BrainVTA), and pAAV-hsyn-EGFP (serotype 2/8, titer $4.66 \times 10^{13}$ v.g./ml; Obio Technology) were injected into the rat MeA [coordinates: antero-posterior (AP) = −2.40 mm; medio-lateral (ML) = ±3.25 mm; dorso-ventral (DV) = −9.10 mm]. pAAV-hsyn-Cre (serotype 2/8, titer $1.30 \times 10^{13}$ v.g./ml; Obio Technology) and pAAV-hsyn-EGFP (serotype 2/8, titer $4.66 \times 10^{13}$ v.g./ml) were injected into the mouse MeA (coordinates: AP = −1.70 mm; ML = ±2.20 mm; DV = −5.20 mm). All the viruses were injected at the amount of 300 nl in rats and 200 nl in mice. Surgical sutures were used to close the skin after surgery. The animals were allowed to recover from anesthesia under a heat lamp before being returned to their home cages, and the animals were allowed to recover for at least 2 weeks before behavioral experiments.

After virus injection, rats were implanted with optical fibers. Each fiber was carefully lowered into the MeA (coordinates: AP = −2.40 mm; ML = ±3.25 mm; DV = −8.90 mm). A small amount of denture powder was sprinkled on the surface of the skull, and a small amount of superglue was applied. Then, water and the denture powder were mixed evenly and laid layer upon layer. After surgery, rats were housed individually to allow full recovery. More details of the optical fiber experiment are shown in the fiber photometry analyses below.

Surgery to implant bilateral guide cannulas at the abovementioned coordinates for drug injection (0.5 μl) was performed under general anesthesia 7 days before the experiments. Injections were performed over 3 min using a Hamilton syringe and a mechanical pump. The injector was left in place for an additional period of 3 min to minimize backflow along the cannula tract. Virus injection and fiber/cannula implantation sites were confirmed post hoc in all animals, and those with incorrect locations were excluded from final analyses.

### Social behavior

The social discrimination tests (*70*, *71*) are varied on the basis of the familiarization and separation time. We applied 24 hours of separation time to study LTSM in rats (*30*). Nonetheless, the LTSM retention of mice has been controversial (*45*, *50*, *54*, *71*), and we tested the optimal separation intervals for mice under our experimental conditions. All experiments were conducted in a dark room, and each test animal was able to distribute its behavior in a three-chamber apparatus. The locations of familiar and novel animals were counterbalanced. We drew regions of interest (ROIs) that were 3 to 5 cm from the edge of the cages to the outer border (*71*). The amount of time spent in the ROIs was recorded by an infrared camera in a dark room.

### Sociability

The animals were tested in a three-chambered apparatus (mice, 20 cm by 45 cm by 20 cm; rats, 120 cm by 40 cm by 20 cm), which contained two metal cages that allow nose contact but prevent fighting (mice, 8-cm diameter by 10-cm height; rats, 8.5 cm by 8.5 cm by 10 cm) in the chambers on each side. Habituation was conducted 24 hours prior for at least 5 min. In the habituation phase, the test animals were familiarized with the empty cage arena, and side preference was measured. The social chamber contained a cage with an unfamiliar male juvenile inside, whereas the object chamber contained a cage with a similar object inside. The animal was placed in the nonpreferred cage.

### Short-term social memory

Test animals were exposed to an unfamiliar juvenile in a novel cage (the same as their home cage) for 5 min. An unfamiliar animal became a familiar one after the interaction. After returning a test animal to its home cage for 30 min of separation, it was then exposed to the familiar animal and a novel animal in the three-chambered apparatus. The familiar animal was placed in the preferred cage determined during sociability.

### Long-term social memory

The protocol of LTSM is similar to STSM except for 1 hour of familiarization and 2 to 24 hours of separation time. The familiar animal was placed in the preferred cage determined during STSM. The LTSM test accompanied photometry recording was conducted in one-half of an open-field apparatus (100 cm by 50 cm by 50 cm) for the free movement of optical fiber.

### Object recognition test

The ORT was conducted in an open-field apparatus consisting of a Plexiglas box (100 cm by 100 cm by 50 cm). At first, rats were gently placed in the center of the arena in a dark room and allowed to explore the area for 5 min in three consecutive days. Next, we prepared two same plastic cylinders (object *A* and *B*, 10 cm by 100 cm) with a hard surface and put them around two axial symmetrical corners of the box separately. The rats were then introduced into the box and allowed to explore the box and objects completely for 10 min. Last, we prepared a cube with a soft surface and similar size to the cylinders (object *C*). Object *A* or *B* (familiar) was randomly replaced by object *C* (novel), and object location is counterbalanced across all conditions. The rats were introduced into the box and tested for 5 min. The experiment was recorded using an infrared camera above the apparatus in a dark room. The time spent exploring the object was scored.

### Elevated plus maze

The EPM apparatus consisted of two open arms (50 cm by 10 cm by 1.5 cm) and two closed arms (50 cm by 10 cm by 35 cm). The apparatus was elevated 50 cm above the floor. Rats were placed at the center of the maze facing the open arm in a dark room and allowed to explore for 5 min. An infrared camera was fixed above the maze and recorded the movement of animals in a dark room. The number of entries into and the time spent in the open arms were scored.

### Open-field test

The open-field apparatus consisted of a Plexiglas box (100 cm by 100 cm by 50 cm). Rats were gently placed in the center of the arena in a dark room and allowed to explore the area for 5 min. The experiment was recorded using an infrared camera above the apparatus in a dark room. The cumulative distance traveled and the time spent in the center (50 cm by 50 cm) were scored.

### Sucrose preference

Rats were housed individually and supplied with two bottles of water and 1% sucrose for 24 hours. After water and food deprivation for 12 hours, the rats were then exposed to a bottle of 1% sucrose and a bottle of water for 12 hours without food. The bottle positions were changed at 6 hours. Sucrose preference was calculated by dividing the total volume of sucrose intake by the total volume of water and sucrose intake.

### Resident-intruder test

A Sprague-Dawley resident male rat (350 to 400 g) was housed with a sexually mature female rat in the resident cage for at least 10 days before the test. Because territoriality is strongly based on the presence of olfactory cues, the bedding of the cages was not cleaned until the test was finished. The companion female was removed 1 hour before behavior evaluation. Subsequently, a Wistar rat (intruder, 350 g) marked on the back was placed into the resident cage. The recording lasted for 10 min with dim light to identify the resident and intruder. The latency to attack and the time spent performing aggression, social, nonsocial, grooming, and static behaviors by the residents were differentiated and measured as previously described (*72*).

### Olfactory habituation/dishabituation test

As previously described (*73*), almond and banana flavors were freshly prepared as the two nonsocial odors, whereas urine and feces were collected on the test day from two different cages of unfamiliar male rats (labeled cage 1 and cage 2) and diluted with a small amount of distilled water as the two social odors. Distilled water was used as a neutral odor. For each trial, a clean applicator was dipped in the odor sample for 2 s. Only the tail end of the applicator was fixed to the edge of the feeding cage, and the head was suspended to avoid any contacts between the smelling tip and the cage. The test session began with three consecutive trials in which the neutral odor was presented, followed by three consecutive trials of the two nonsocial odors and the two social odors for 2 min per trial. The intertrial interval was 1 to 2 min, during which the applicators were removed and dropped into an airtight bin, and the next trial was prepared. The entire process was video-recorded to measure the time in zone around the applicator heads.

### Fiber photometry analyses

Fiber photometry recording was performed as previously described (*74*, *75*) with a commercialized fiber photometry system (model FIS, ThinkerTech). The pAAV-hsyn-GCaMP6s was stereotaxically injected into the MeA of WT and OXTR S261A$^{+/+}$ knock-in rats, followed by the implantation of optical fiber [optical density (OD) = 200 mm; numerical aperture (NA) = 0.37] placed in a ceramic ferrule (OD = 2.5 mm) by craniotomy. Fiber recordings were performed in freely moving rats 2 weeks after virus injection. To induce fluorescence signals, a laser beam from a laser tube (488 nm) was reflected by a dichroic mirror focused by a 10× lens (NA = 0.3) and coupled to an optical commutator. An optical fiber (OD = 200 mm; NA = 0.37; length = 2 to 3 m) guided the light between the commutator and the implanted optical fiber. The laser power was adjusted at the tip of the optical fiber to a low level of 30 to 40 mW to minimize the bleaching of the GCaMP6s probes. The GCaMP6s fluorescence was band-pass–filtered (MF525-39, Thorlabs) and collected by a photomultiplier tube (R3896, Hamamatsu, Japan). An amplifier (C7319, Hamamatsu) was used to convert the photomultiplier tube current output to voltage signals, which was further filtered through a low-pass filter (40-Hz cutoff; Brownlee 440). The analog voltage signals were digitalized at 100 Hz and recorded by a Power 1401 digitizer. Photometry data were exported as MATLAB files for further analysis. The baseline time window for $\Delta F/F$ calculations is 2 s before each social interaction onset. To calculate the averaged bouts of animals, the mean value for each animal was calculated first, followed by analysis between different animals.

### Quantification and statistical analysis

The sample size was determined according to the accepted practice for behavioral assays, but no statistical methods were used to predetermine sample size. Experiments and analyses were performed in a blinded manner. Statistical analyses were performed with GraphPad Prism 7.0 or MATLAB_R2014b. The data were first tested for normality. If the null hypothesis that the data come from a normal distribution cannot be rejected, Student's *t* test was used in a two-group comparison, and Welch's correction was used when the *F* test showed a significant difference. For multiple-group comparison, one-way analysis of variance (ANOVA) was used with Tukey's post hoc test and two-way ANOVA with Sidak's post hoc test. If the data did not follow a normal distribution, Mann-Whitney test was used in the two-group comparison. The behaviors were all analyzed by Smart v3.03 by either automatic detection (social behaviors, ORT, OFT, and EPM) or manual detection (resident-intruder test and olfactory

test). To evaluate the sniffing/exploring time in the social behaviors and ORT, we drew ROIs that were 3 to 5 cm from the edge of the cages or objects to the outer border (*71*). Cumulative time was scored when the head of the animal was detected in the ROIs. The heatmaps of social memory were drawn by EthoVision XT. All data are expressed as the means ± SEM, with $n$ indicating the number of experiments or animals analyzed. $P < 0.05$ was considered statistically significant.

## SUPPLEMENTARY MATERIALS

www.science.org/doi/10.1126/scisignal.abd0033
Figs. S1 to S6
Table S1
Movie S1

View/request a protocol for this paper from *Bio-protocol*.

## REFERENCES AND NOTES


1. B. J. Crespi, T. L. Procyshyn, Williams syndrome deletions and duplications: Genetic windows to understanding anxiety, sociality, autism, and schizophrenia. *Neurosci. Biobehav. Rev.* **79**, 14–26 (2017).
2. I. Cataldo, A. Azhari, G. Esposito, A review of oxytocin and arginine-vasopressin receptors and their modulation of autism spectrum disorder. *Front. Mol. Neurosci.* **11**, 27 (2018).
3. L. A. McGraw, L. J. Young, The prairie vole: An emerging model organism for understanding the social brain. *Trends Neurosci.* **33**, 103–109 (2010).
4. T. Okuyama, Social memory engram in the hippocampus. *Neurosci. Res.* **129**, 17–23 (2018).
5. M. Mitre, B. J. Marlin, J. K. Schiavo, E. Morina, S. E. Norden, T. A. Hackett, C. J. Aoki, M. V. Chao, R. C. Froemke, A distributed network for social cognition enriched for oxytocin receptors. *J. Neurosci.* **36**, 2517–2535 (2016).
6. B. Jurek, I. D. Neumann, The oxytocin receptor: From intracellular signaling to behavior. *Physiol. Rev.* **98**, 1805–1908 (2018).
7. T. Raam, K. M. McAvoy, A. Besnard, A. H. Veenema, A. Sahay, Hippocampal oxytocin receptors are necessary for discrimination of social stimuli. *Nat. Commun.* **8**, 2001 (2017).
8. N. Duque-Wilckens, L. Y. Torres, S. Yokoyama, V. A. Minie, A. M. Tran, S. P. Petkova, R. Hao, S. Ramos-Maciel, R. A. Rios, K. Jackson, F. J. Flores-Ramirez, I. Garcia-Carachure, P. A. Pesavento, S. D. Iniguez, V. Grinevich, B. C. Trainor, Extrahypothalamic oxytocin neurons drive stress-induced social vigilance and avoidance. *Proc. Natl. Acad. Sci. U.S.A.* **117**, 26406–26413 (2020).
9. S. Anpilov, Y. Shemesh, N. Eren, H. Harony-Nicolas, A. Benjamin, J. Dine, V. E. M. Oliveira, O. Forkosh, S. Karamihalev, R. E. Huttl, N. Feldman, R. Berger, A. Dagan, G. Chen, I. D. Neumann, S. Wagner, O. Yizhar, A. Chen, Wireless optogenetic stimulation of oxytocin neurons in a semi-natural setup dynamically elevates both pro-social and agonistic behaviors. *Neuron* **107**, 644–655.e7 (2020).
10. K. Berrada, C. L. Plesnicher, X. Luo, M. Thibonnier, Dynamic interaction of human vasopressin/oxytocin receptor subtypes with G protein-coupled receptor kinases and protein kinase C after agonist stimulation. *J. Biol. Chem.* **275**, 27229–27237 (2000).
11. G. Gimpl, F. Fahrenholz, The oxytocin receptor system: Structure, function, and regulation. *Physiol. Rev.* **81**, 629–683 (2001).
12. C. A. Grotegut, L. Feng, L. Mao, R. P. Heine, A. P. Murtha, H. A. Rockman, β-Arrestin mediates oxytocin receptor signaling, which regulates uterine contractility and cellular migration. *Am. J. Physiol. Endocrinol. Metab.* **300**, E468–E477 (2011).
13. M. Busnelli, A. Saulière, M. Manning, M. Bouvier, C. Gales, B. Chini, Functional selective oxytocin-derived agonists discriminate between individual G protein family subtypes. *J. Biol. Chem.* **287**, 3617–3629 (2012).
14. K. Tomizawa, N. Iga, Y. F. Lu, A. Moriwaki, M. Matsushita, S. T. Li, O. Miyamoto, T. Itano, H. Matsui, Oxytocin improves long-lasting spatial memory during motherhood through MAP kinase cascade. *Nat. Neurosci.* **6**, 384–390 (2003).
15. Y. Satoh, S. Endo, T. Nakata, Y. Kobayashi, K. Yamada, T. Ikeda, A. Takeuchi, T. Hiramoto, Y. Watanabe, T. Kazama, ERK2 contributes to the control of social behaviors in mice. *J. Neurosci.* **31**, 11953–11967 (2011).
16. L. Norskov-Lauritsen, H. Bräuner-Osborne, Role of post-translational modifications on structure, function and pharmacology of class C G protein-coupled receptors. *Eur. J. Pharmacol.* **763**, 233–240 (2015).
17. R. Prihandoko, S. J. Bradley, A. B. Tobin, A. J. Butcher, Determination of GPCR phosphorylation status: Establishing a phosphorylation barcode. *Curr. Protoc. Pharmacol.* **69**, 2.13.1–2.13.26 (2015).
18. F. J. Johannes, J. Prestle, S. Eis, P. Oberhagemann, K. Pfizenmaier, PKCu is a novel, atypical member of the protein kinase C family. *J. Biol. Chem.* **269**, 6140–6148 (1994).
19. M. Bisbal, C. Conde, M. Donoso, F. Bollati, J. Sesma, S. Quiroga, A. Diaz Anel, V. Malhotra, M. P. Marzolo, A. Caceres, Protein kinase d regulates trafficking of dendritic membrane proteins in developing neurons. *J. Neurosci.* **28**, 9297–9308 (2008).
20. D.-M. Yin, Y.-H. Huang, Y.-B. Zhu, Y. Wang, Both the establishment and maintenance of neuronal polarity require the activity of protein kinase D in the Golgi apparatus. *J. Neurosci.* **28**, 8832–8843 (2008).
21. K. Czondor, K. Ellwanger, Y. F. Fuchs, S. Lutz, M. Gulyas, I. M. Mansuy, A. Hausser, K. Pfizenmaier, K. Schlett, Protein kinase D controls the integrity of Golgi apparatus and the maintenance of dendritic arborization in hippocampal neurons. *Mol. Biol. Cell* **20**, 2108–2120 (2009).
22. N. Bencsik, Z. Sziber, H. Liliom, K. Tarnok, S. Borbely, M. Gulyas, A. Ratkai, A. Szucs, D. Hazai-Novak, K. Ellwanger, B. Racz, K. Pfizenmaier, A. Hausser, K. Schlett, Protein kinase D promotes plasticity-induced F-actin stabilization in dendritic spines and regulates memory formation. *J. Cell Biol.* **210**, 771–783 (2015).
23. C. Cen, L. D. Luo, W. Q. Li, G. Li, N. X. Tian, G. Zheng, D. M. Yin, Y. Zou, Y. Wang, PKD1 promotes functional synapse formation coordinated with N-cadherin in hippocampus. *J. Neurosci.* **38**, 183–199 (2018).
24. E. Rozengurt, Protein kinase D signaling: Multiple biological functions in health and disease. *Physiology* **26**, 23–33 (2011).
25. N. Wang, P. Su, Y. Zhang, J. Lu, B. Xing, K. Kang, W. Li, Y. Wang, Protein kinase D1-dependent phosphorylation of dopamine D1 receptor regulates cocaine-induced behavioral responses. *Neuropsychopharmacology* **39**, 1290–1301 (2014).
26. C. McCall, T. Singer, The animal and human neuroendocrinology of social cognition, motivation and behavior. *Nat. Neurosci.* **15**, 681–688 (2012).
27. I. D. Neumann, D. A. Slattery, Oxytocin in general anxiety and social fear: A translational approach. *Biol. Psychiatry* **79**, 213–221 (2016).
28. A. Blume, O. J. Bosch, S. Miklos, L. Torner, L. Wales, M. Waldherr, I. D. Neumann, Oxytocin reduces anxiety via ERK1/2 activation: Local effect within the rat hypothalamic paraventricular nucleus. *Eur. J. Neurosci.* **27**, 1947–1956 (2008).
29. B. Jurek, D. A. Slattery, R. Maloumby, K. Hillerer, S. Koszinowski, I. D. Neumann, E. H. van den Burg, Differential contribution of hypothalamic MAPK activity to anxiety-like behaviour in virgin and lactating rats. *PLOS ONE* **7**, e37060 (2012).
30. R. Gur, A. Tendler, S. Wagner, Long-term social recognition memory is mediated by oxytocin-dependent synaptic plasticity in the medial amygdala. *Biol. Psychiatry* **76**, 377–386 (2014).
31. T. Lüscher Dias, H. Fernandes Golino, V. E. Moura de Oliveira, M. F. Dutra Moraes, G. S. Pereira, c-Fos expression predicts long-term social memory retrieval in mice. *Behav. Brain Res.* **313**, 260–271 (2016).
32. J. N. Ferguson, J. M. Aldag, T. R. Insel, L. J. Young, Oxytocin in the medial amygdala is essential for social recognition in the mouse. *J. Neurosci.* **21**, 8278–8285 (2001).
33. G. Gimpl, J. Reitz, S. Brauer, C. Trossen, Oxytocin receptors: Ligand binding, signalling and cholesterol dependence. *Prog. Brain Res.* **170**, 193–204 (2008).
34. V. O. Rybin, J. Guo, E. Harleton, F. Zhang, S. F. Steinberg, Regulatory domain determinants that control PKD1 activity. *J. Biol. Chem.* **287**, 22609–22615 (2012).
35. V. O. Rybin, J. Guo, S. F. Steinberg, Protein kinase D1 autophosphorylation via distinct mechanisms at $Ser^{744}$/$Ser^{748}$ and $Ser^{916}$. *J. Biol. Chem.* **284**, 2332–2343 (2009).
36. E. Rozengurt, O. Rey, R. T. Waldron, Protein kinase D signaling. *J. Biol. Chem.* **280**, 13205–13208 (2005).
37. M. Lukas, I. Toth, A. H. Veenema, I. D. Neumann, Oxytocin mediates rodent social memory within the lateral septum and the medial amygdala depending on the relevance of the social stimulus: Male juvenile versus female adult conspecifics. *Psychoneuroendocrinology* **38**, 916–926 (2013).
38. J. Seo, K.-J. Lee, Post-translational modifications and their biological functions: Proteomic analysis and systematic approaches. *J. Biochem. Mol. Biol.* **37**, 35–44 (2004).
39. D. Wootten, A. Christopoulos, M. Marti-Solano, M. M. Babu, P. M. Sexton, Mechanisms of signalling and biased agonism in G protein-coupled receptors. *Nat. Rev. Mol. Cell Biol.* **19**, 638–653 (2018).
40. T. Kimura, Y. Makino, R. Bathgate, R. Ivell, T. Nobunaga, Y. Kubota, I. Kumazawa, F. Saji, Y. Murata, T. Nishihara, M. Hashimoto, M. Kinoshita, The role of N-terminal glycosylation in the human oxytocin receptor. *Mol. Hum. Reprod.* **3**, 957–963 (1997).
41. R. Schülein, U. Liebenhoff, H. Müller, M. Birnbaumer, W. Rosenthal, Properties of the human arginine vasopressin V2 receptor after site-directed mutagenesis of its putative palmitoylation site. *Biochem. J.* **313** (Pt. 2), 611–616 (1996).
42. A. Hasbi, D. Devost, S. A. Laporte, H. H. Zingg, Real-time detection of interactions between the human oxytocin receptor and G protein-coupled receptor kinase-2. *Mol. Endocrinol.* **18**, 1277–1286 (2004).
43. M. P. Smith, V. J. Ayad, S. J. Mundell, C. A. McArdle, E. Kelly, A. L. Bernal, Internalization and desensitization of the oxytocin receptor is inhibited by Dynamin and clathrin mutants in human embryonic kidney 293 cells. *Mol. Endocrinol.* **20**, 379–388 (2006).
44. F. L. Hitti, S. A. Siegelbaum, The hippocampal CA2 region is essential for social memory. *Nature* **508**, 88–92 (2014).

45. T. Okuyama, T. Kitamura, D. S. Roy, S. Itohara, S. Tonegawa, Ventral CA1 neurons store social memory. *Science* **353**, 1536–1541 (2016).
46. M.-C. Chiang, A. J. Y. Huang, M. E. Wintzer, T. Ohshima, T. J. McHugh, A role for CA3 in social recognition memory. *Behav. Brain Res.* **354**, 22–30 (2018).
47. T. Meira, F. Leroy, E. W. Buss, A. Oliva, J. Park, S. A. Siegelbaum, A hippocampal circuit linking dorsal CA2 to ventral CA1 critical for social memory dynamics. *Nat. Commun.* **9**, 4163 (2018).
48. F. Leroy, C. A. de Solis, L. M. Boyle, T. Bock, O. M. Lofaro, E. W. Buss, A. Asok, E. R. Kandel, S. A. Siegelbaum, Enkephalin release from VIP interneurons in the hippocampal CA2/3a region mediates heterosynaptic plasticity and social memory. *Mol. Psychiatry* , (2021).
49. B. Xing, N. R. Mack, K.-M. Guo, Y.-X. Zhang, B. Ramirez, S.-S. Yang, L. Lin, D. V. Wang, Y.-C. Li, W.-J. Gao, A subpopulation of prefrontal cortical neurons is required for social memory. *Biol. Psychiatry* **89**, 521–531 (2021).
50. Y. T. Lin, T. Y. Hsieh, T. C. Tsai, C. C. Chen, C. C. Huang, K. S. Hsu, Conditional deletion of hippocampal CA2/CA3a oxytocin receptors impairs the persistence of long-term social recognition memory in mice. *J. Neurosci.* **38**, 1218–1231 (2018).
51. M. Luo, M. S. Fee, L. C. Katz, Encoding pheromonal signals in the accessory olfactory bulb of behaving mice. *Science* **299**, 1196–1201 (2003).
52. D. Y. Lin, S. Z. Zhang, E. Block, L. C. Katz, Encoding social signals in the mouse main olfactory bulb. *Nature* **434**, 470–477 (2005).
53. S. Keshavarzi, J. M. Power, E. H. Albers, R. K. Sullivan, P. Sah, Dendritic organization of olfactory inputs to medial amygdala neurons. *J. Neurosci.* **35**, 13020–13028 (2015).
54. T. Tanimizu, J. W. Kenney, E. Okano, K. Kadoma, P. W. Frankland, S. Kida, Functional connectivity of multiple brain regions required for the consolidation of social recognition memory. *J. Neurosci.* **37**, 4103–4116 (2017).
55. S. Yao, J. Bergan, A. Lanjuin, C. Dulac, Oxytocin signaling in the medial amygdala is required for sex discrimination of social cues. *eLife* **6**, e31373 (2017).
56. N. V. Kukushkin, T. J. Carew, Memory takes time. *Neuron* **95**, 259–279 (2017).
57. D. Norris, Short-term memory and long-term memory are still different. *Psychol. Bull.* **143**, 992–1009 (2017).
58. K. Richter, G. Wolf, M. Engelmann, Social recognition memory requires two stages of protein synthesis in mice. *Learn. Mem.* **12**, 407–413 (2005).
59. R. R. Pena, A. R. Pereira-Caixeta, M. F. Moraes, G. S. Pereira, Anisomycin administered in the olfactory bulb and dorsal hippocampus impaired social recognition memory consolidation in different time-points. *Brain Res. Bull.* **109**, 151–157 (2014).
60. B. N. Kholodenko, Cell-signalling dynamics in time and space. *Nat. Rev. Mol. Cell Biol.* **7**, 165–176 (2006).
61. J. Sebat, B. Lakshmi, D. Malhotra, J. Troge, C. Lese-Martin, T. Walsh, B. Yamrom, S. Yoon, A. Krasnitz, J. Kendall, A. Leotta, D. Pai, R. Zhang, Y. H. Lee, J. Hicks, S. J. Spence, A. T. Lee, K. Puura, T. Lehtimaki, D. Ledbetter, P. K. Gregersen, J. Bregman, J. S. Sutcliffe, V. Jobanputra, W. Chung, D. Warburton, M. C. King, D. Skuse, D. H. Geschwind, T. C. Gilliam, K. Ye, M. Wigler, Strong association of de novo copy number mutations with autism. *Science* **316**, 445–449 (2007).
62. D. Feifel, P. D. Shilling, K. MacDonald, A review of oxytocin's effects on the positive, negative, and cognitive domains of schizophrenia. *Biol. Psychiatry* **79**, 222–233 (2016).
63. M. G. Gottschalk, K. Domschke, Oxytocin and anxiety disorders. *Curr. Top Behav. Neurosci.* **35**, 467–498 (2018).
64. M. E. Persson, A. J. Trottier, J. Belteky, L. S. V. Roth, P. Jensen, Intranasal oxytocin and a polymorphism in the oxytocin receptor gene are associated with human-directed social behavior in golden retriever dogs. *Horm. Behav.* **95**, 85–93 (2017).
65. H. Kosaka, Y. Okamoto, T. Munesue, H. Yamasue, K. Inohara, T. Fujioka, T. Anme, M. Orisaka, M. Ishitobi, M. Jung, T. X. Fujisawa, S. Tanaka, S. Arai, M. Asano, D. N. Saito, N. Sadato, A. Tomoda, M. Omori, M. Sato, H. Okazawa, H. Higashida, Y. Wada, Oxytocin efficacy is modulated by dosage and oxytocin receptor genotype in young adults with high-functioning autism: A 24-week randomized clinical trial. *Transl. Psychiatry* **6**, e872 (2016).
66. S. H. Seeley, Y. H. Chou, M. F. O'Connor, Intranasal oxytocin and OXTR genotype effects on resting state functional connectivity: A systematic review. *Neurosci. Biobehav. Rev.* **95**, 17–32 (2018).
67. G. Leng, M. Ludwig, Intranasal Oxytocin: Myths and delusions. *Biol. Psychiatry* **79**, 243–250 (2016).
68. H. Walum, I. D. Waldman, L. J. Young, Statistical and methodological considerations for the interpretation of intranasal oxytocin studies. *Biol. Psychiatry* **79**, 251–257 (2016).
69. S. Benner, Y. Aoki, T. Watanabe, N. Endo, O. Abe, M. Kuroda, H. Kuwabara, Y. Kawakubo, H. Takao, A. Kunimatsu, K. Kasai, H. Bito, M. Kakeyama, H. Yamasue, Neurochemical evidence for differential effects of acute and repeated oxytocin administration. *Mol. Psychiatry* **26**, 710–720 (2018).
70. M. Engelmann, C. T. Wotjak, R. Landgraf, Social discrimination procedure: An alternative method to investigate juvenile recognition abilities in rats. *Physiol. Behav.* **58**, 315–321 (1995).
71. A. Zimprich, J. Niessing, L. Cohen, L. Garrett, J. Einicke, B. Sperling, M. V. Schmidt, S. M. Holter, Assessing sociability, social memory, and pup retrieval in mice. *Curr. Protoc. Mouse Biol.* **7**, 287–305 (2017).
72. J. M. Koolhaas, C. M. Coppens, S. F. de Boer, B. Buwalda, P. Meerlo, P. J. Timmermans, The resident-intruder paradigm: A standardized test for aggression, violence and social stress. *J. Vis. Exp.* , e4367 (2013).
73. R. M. Witt, M. M. Galligan, J. R. Despinoy, R. Segal, Olfactory behavioral testing in the adult mouse. *J. Vis. Exp.* , 949 (2009).
74. Y. Li, W. Zhong, D. Wang, Q. Feng, Z. Liu, J. Zhou, C. Jia, F. Hu, J. Zeng, Q. Guo, L. Fu, M. Luo, Serotonin neurons in the dorsal raphe nucleus encode reward signals. *Nat. Commun.* **7**, 10503 (2016).
75. D. Wang, Y. Li, Q. Feng, Q. Guo, J. Zhou, M. Luo, Learning shapes the aversion and reward responses of lateral habenula neurons. *eLife* **6**, e23045 (2017).


**Acknowledgments:** We thank M. Luo at National Institute of Biological Sciences for helping with the statistical analysis of fiber photometry. **Funding:** This work was supported by grants from the Ministry of Science and Technology of China (2021ZD0203204 to Y.W.) and grants from the National Natural Science Foundation of China (31530028 to Y.W., 81873738 to C.C., and 31720103908 and 81821092 to Y.W.). **Author contributions:** Study conceptualized by F.W., J.L., and Y.W.; methodology devised by F.W. and J.L.; experiments performed by F.W., X.-S.Y., and J.L.; original manuscript drafted by F.W. and X.-S.Y.; manuscript revised by F.W., X.-S.Y., C.C., and Y.W.; funding acquired by C.C. and Y.W.; resources provided by F.W., J.L., and Y.W.; and study supervised by C.C. and Y.W. **Competing interests:** The authors declare that they have no competing interests. **Data and materials availability:** All data needed to evaluate the conclusions in the paper are present in the paper or the Supplementary Materials. Codes and strains associated with this work are available upon request.

Submitted 26 May 2020
Resubmitted 19 July 2021
Accepted 20 December 2021
Published 1 February 2022
10.1126/scisignal.abd0033

Science Signaling

# Phosphorylation-dependent positive feedback on the oxytocin receptor through the kinase PKD1 contributes to long-term social memory

Fei Wang, Xiang-Sha Yin, Jie Lu, Cheng Cen, and Yun Wang

*Sci. Signal.*, **15** (719), eabd0033.
DOI: 10.1126/scisignal.abd0033

**Familiarity feedback**

Social memory enables the recognition of others and the formation and maintenance of relationships and thus regulates social behaviors. It is in part supported by the bonding hormone oxytocin. Wang *et al.* found that an oxytocin receptor–dependent positive feedback loop contributes to long-term social memory in rodents. Reciprocal phosphorylation between the receptor and the kinase PKD1 promoted downstream oxytocin receptor signaling in cultured cells. Rodents in which this loop was disrupted in the medial amygdala of the brain showed behaviors and neuronal activity that indicated impaired recognition of familiar cage mates. The findings provide molecular and physiological insight on how oxytocin signaling promotes social memory.



*Science Signaling* (ISSN ) is published by the American Association for the Advancement of Science. 1200 New York Avenue NW, Washington, DC 20005. The title *Science Signaling* is a registered trademark of AAAS.